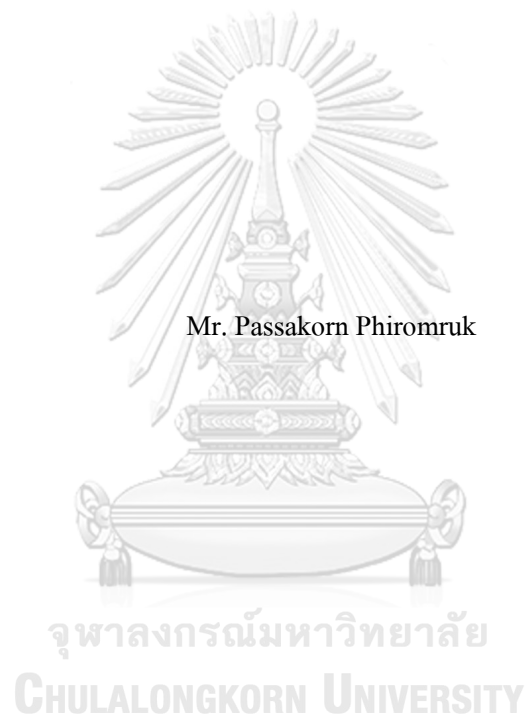


FABRICATION AND CHARACTERIZATION OF TRIPLE-CATION PEROVSKITE SOLAR  
CELLS



A Thesis Submitted in Partial Fulfillment of the Requirements

for the Degree of Master of Science in Physics

Department of Physics

FACULTY OF SCIENCE

Chulalongkorn University

Academic Year 2020

Copyright of Chulalongkorn University

การประดิษฐ์และการหาลักษณะเฉพาะของเซลล์สุริยะเพอรอฟสไกต์ไอออนบวกสามชนิด



วิทยานิพนธ์นี้เป็นส่วนหนึ่งของการศึกษาตามหลักสูตรปริญญาวิทยาศาสตรมหาบัณฑิต  
สาขาวิชาฟิสิกส์ ภาควิชาฟิสิกส์  
คณะวิทยาศาสตร์ จุฬาลงกรณ์มหาวิทยาลัย  
ปีการศึกษา 2563  
ลิขสิทธิ์ของจุฬาลงกรณ์มหาวิทยาลัย



ภาสกร ภิรมณ์รัก : การประดิษฐ์และการหาลักษณะเฉพาะของเซลล์สุริยะเพอโรฟสไกต์ไอออนบวกสามชนิด . ( FABRICATION AND CHARACTERIZATION OF TRIPLE-CATION PEROVSKITE SOLAR CELLS) อ.ที่ปรึกษาหลัก : ผศ. ดร. โสจิพงศ์ ฉัตรภรณ์

ในปัจจุบันเซลล์สุริยะเพอโรฟสไกต์ไอออนบวกสามชนิดเป็นที่น่าสนใจเนื่องจากความโดดเด่นทั้งทางด้านประสิทธิภาพและความเสถียรเมื่อเทียบกับเซลล์สุริยะเพอโรฟสไกต์ตัวอื่น ๆ ในงานวิจัยนี้ เซลล์สุริยะ  $\text{Cs}_{0.03}(\text{FA}_x\text{MA}_{1-x})_{0.97}\text{Pb}(\text{I}_y\text{Br}_{1-y})_3$  จะถูกปลูกด้วยวิธีการปลูกแบบสองขั้นตอน (two-step deposition) โดยศึกษาผลของปริมาณของไอออนบวกและปริมาณของไอออนหมู่ 7 จากผลการทดลอง พบว่าการเพิ่มโบรมไนด์เข้าไปจะส่งผลให้ค่าความต่างศักย์วงจรเปิด ( $V_{oc}$ ) มีค่าสูงขึ้น ซึ่งเป็นผลมาจากค่าช่องว่างพลังงานที่เพิ่มสูงขึ้น และสำหรับกรณีของเซลล์ที่ประกอบด้วย  $\text{MAPbI}_3$  ส่วนใหญ่ ได้ค่าประสิทธิภาพที่ดีขึ้นเมื่อโบรมไนด์ถูกเพิ่มเข้าไป แต่ประสิทธิภาพของเซลล์ที่ประกอบด้วย  $\text{FAPbI}_3$  เป็นส่วนใหญ่ มีประสิทธิภาพที่ต่ำกว่าเนื่องจากคุณภาพของฟิล์มเพอโรฟสไกต์ที่แยกและเชื่อมไม่สามารถทำให้เฟสดีค่าของ  $\text{FAPbI}_3$  เสถียร ดังนั้นกระบวนการปลูกแบบสองขั้นตอนแบบมีเพอโรฟสไกต์ซิด (two-step deposition method with perovskite seeds) จึงถูกนำมาใช้สำหรับเซลล์ที่ประกอบด้วย  $\text{FAPbI}_3$  เป็นส่วนใหญ่ กระบวนการนี้ต่างจากกระบวนการปลูกแบบสองขั้นตอนเล็กน้อย โดยการเติมเพอโรฟสไกต์ซิดเข้าไปในสารละลาย  $\text{PbI}_2$  โดยเมื่อสังเกตภาพจากกล้องจุลทรรศน์อิเล็กตรอนแบบส่องกราด พบว่าพื้นผิวฟิล์มที่ได้จะมีช่องว่างระหว่างฟิล์มน้อยลงเมื่อใช้กระบวนการปลูกแบบใหม่ และช่วยปรับปรุงพื้นผิวระหว่างชั้นเพอโรฟสไกต์กับชั้น Spiro-MeOTAD โดยค่าประสิทธิภาพเฉลี่ยเพิ่มขึ้นจากเดิม 5.2% ไปยัง 11.9% เมื่อเปลี่ยนกระบวนการปลูกเป็นกระบวนการใหม่ เพราะพื้นผิวฟิล์มเพอโรฟสไกต์ที่ดีขึ้นและซิดช่วยสร้างการเกิดผลึกได้ดีขึ้น ดังนั้น ในการปลูกเซลล์ประกอบประกอบด้วย  $\text{FAPbI}_3$  เป็นส่วนใหญ่ให้มีประสิทธิภาพที่สูงจำเป็นต้องใช้ขั้นตอนต่าง ๆ เพิ่มขึ้น เช่น การนำเพอโรฟสไกต์ซิดมาใช้ นอกจากนี้กระบวนการใหม่นี้ยังช่วยให้ประสิทธิภาพของเซลล์ที่ได้มีค่าสูงขึ้นเมื่อเปลี่ยนปริมาณคลอโรเบนซีน เช่น ค่าประสิทธิภาพเฉลี่ยของเซลล์ที่ปลูกด้วยกระบวนการใหม่และซิดมีความเข้มข้นเป็น 14% v/v มีค่าเพิ่มขึ้นจาก 10.8% เป็น 14.3% เมื่อปริมาณของคลอโรเบนซีนลดลงจาก 50 เป็น 30 ไมโครลิตร นอกจากนี้ประสิทธิภาพของเซลล์มาตรฐาน  $\text{MAPbI}_3$  ถูกนำมาเปรียบเทียบกับเซลล์สุริยะเพอโรฟสไกต์ไอออนบวกสามชนิดที่ถูกปลูกด้วยสองวิธีการข้างต้น จากผลการทดลอง พบว่าขนาดของผลึกเพอโรฟสไกต์ไม่ได้เป็นปัจจัยสำคัญในการบ่งบอกถึงประสิทธิภาพของเซลล์ เพราะค่าประสิทธิภาพเฉลี่ยของตัวมาตรฐานและเซลล์ประกอบประกอบด้วย  $\text{FAPbI}_3$  เป็นส่วนใหญ่จากกระบวนการปลูกแบบใหม่ ให้ค่าประสิทธิภาพที่ใกล้เคียงกัน แม้ว่าขนาดผลึกของ  $\text{FAPbI}_3$  จะมีขนาดเล็กกว่าอย่างเห็นได้ชัด

สาขาวิชา      ฟิสิกส์  
ปีการศึกษา      2563

ลายมือชื่อนิติศ .....  
ลายมือชื่อ อ.ที่ปรึกษาหลัก .....

## 6172034023 : MAJOR PHYSICS

KEYWORD:

Passakorn Phiromruk : FABRICATION AND CHARACTERIZATION OF TRIPLE-CATION PEROVSKITE SOLAR CELLS. Advisor: Asst. Prof. SOJIPHONG CHATRAPHORN, Ph.D.

Presently, triple-cation perovskite solar cells have been appealing due to the outstanding power conversion efficiency (PCE). In this work, the  $\text{Cs}_{0.03}(\text{FA}_x\text{MA}_{1-x})_{0.97}\text{Pb}(\text{I}_y\text{Br}_{1-y})_3$  triple-cation perovskite solar cells fabricated by two-step deposition method were studied by varying the content of halide ions (Br and I) and the cation ratios of FA and MA. The results showed that the insertion of Br improved open-circuit voltage due to broader band gap. In case of  $\text{MAPbI}_3$ -based devices, the PCE was also increased with the addition of Br. However, the  $\text{FAPbI}_3$ -based devices were inferior to  $\text{MAPbI}_3$ -based devices resulting from poor quality perovskite layer and the non-photoactive structure of  $\text{FAPbI}_3$ . To fabricate the  $\text{FAPbI}_3$ -based devices, more procedures were needed to obtain high performance. Two-step deposition method with perovskite seeds was employed to improve the photovoltaic performance of  $\text{FAPbI}_3$ -based devices. This process was slightly modified from conventional two-step deposition methods by adding small amount of perovskite seed precursor into  $\text{PbI}_2$  solution and the concentration of the perovskite seeds in  $\text{PbI}_2$  solution was varied in this study. The SEM images indicated that the  $\text{FAPbI}_3$ -based films of the new method were more compact and denser than that of the conventional method which improved surface coverage causing the better contact between perovskite layer and hole transport layer. The average PCEs were enhanced from 5.2% to 11.9% when the fabrication method changed from the conventional method to two-step deposition method with 7% v/v seeding concentration due to the favorable of perovskite seeds for crystal formation and improved contact of photoactive layer and hole transport layer. The performance of the seeding method could be improved by using proper amount of chlorobenzene as an anti-solvent. For instance, the average PCEs of 14% v/v seeding concentration was risen from 10.8% to 14.3% when the applied anti-solvent was changed from 50  $\mu\text{l}$  to 30  $\mu\text{l}$ . Besides, the photovoltaic performance of triple-cation perovskite solar cells from both methods and the standard  $\text{MAPbI}_3$  were compared. It was found that the grain size was not an impact factor to determine the performance of devices because the average PCEs of seeded devices were around 13-14% as much as the standard devices and  $\text{MAPbI}_3$ -based devices, although the grain size of  $\text{FAPbI}_3$ - and  $\text{MAPbI}_3$ -based devices were noticeably different.

Field of Study:            Physics

Student's Signature .....

Academic Year:        2020

Advisor's Signature .....

## ACKNOWLEDGEMENTS

I would like to express my gratitude to my thesis advisor, Assistant Professor Dr. Sojiphong Chatraphorn, for your kind advice, criticism, and motivation. His navigation and knowledge helped me to immensely improve my work and my thesis. Also, I would like to thank my thesis committee, Assistant Professor Dr. Thiti Taychatanaphat, Associate Professor Dr. Udomsilp Pinsook, and Associate Professor Dr. Rachask Sakdanuphab for their comments and suggestions.

I would like to thank to Mr. Pornsak Panchawirat for his help of SEM measurement and Dr. Boonyaluk Namnuan for her help with technical suggestion in this work. Besides, I would like to thank you Ms. Kwanruthai Butsriruk for her help and suggestion to the experiment.

I could not thank enough to my colleague and friend, Rattanaporn Thanimkan, for her help with studying and assisting the experiment. Moreover, I would like to thank to my friends who studied with me in the classes, Narongkiat Rodphai and Illias Klanurak, for their helps and entertaining.

I would like to also thank my best friends, namely, Siriwan, Anutida, Chiratt, Thanasinee, Yordchart, for their kind support. I would have had mental breakdown without these people. Furthermore, I would like to thank Samagorn and Narongkiat for hanging out and drinking with me most of the time.

Finally, I would like to express my appreciation to my family for their support especially my sister who helped me get through at the rough time.

Passakorn Phiromruk

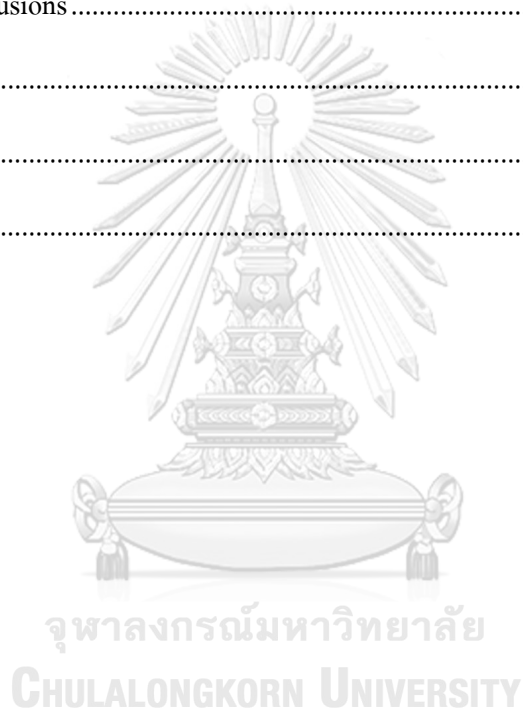
## TABLE OF CONTENTS

	<b>Page</b>
.....	iii
ABSTRACT (THAI).....	iii
.....	iv
ABSTRACT (ENGLISH).....	iv
ACKNOWLEDGEMENTS.....	v
TABLE OF CONTENTS.....	vi
LIST OF TABLES.....	ix
LIST OF FIGURES.....	x
Chapter I Introduction.....	1
1.1 Overview.....	1
1.2 A brief history of perovskite.....	2
1.3 Triple-cation perovskite solar cells.....	4
1.4 Objectives.....	5
1.5 Thesis outlines.....	6
Chapter II Basics of semiconductor, solar cells, and perovskite solar cells.....	7
2.1 Perovskite structure.....	7
2.2 Perovskite fabrication.....	8
2.3 Band gap energy.....	9
2.4 P-N junction.....	11
2.5 Perovskite solar cell structure.....	13
2.5.1 Front contact.....	14

2.5.2 Electron transport layer or blocking layer.....	14
2.5.3 Photoactive layer.....	15
2.5.4 Hole transport layer.....	15
2.5.5 Back contact.....	15
2.6 Solar cell parameters .....	15
Chapter III Fabrication and Characterization.....	19
3.1 Preparation of substrates and materials for perovskite solar cells .....	19
3.1.1 Front contact .....	19
3.1.2 Electron transport layer(s).....	19
3.1.3 Absorber layer.....	20
3.1.3.1 Two-step deposition method.....	20
3.1.3.2 Two-step deposition method with perovskite seeds .....	21
3.1.4 Hole transport layer.....	21
3.2 Deposition processes of each layer for perovskite solar cells.....	21
3.3 Characterization of perovskite solar cells .....	22
3.3.1 Percent transmission .....	23
3.3.2 The calculation of optical band gap .....	23
3.3.3 Scanning electron microscopy .....	24
3.3.4 J-V characteristics .....	25
Chapter IV Results and Discussion.....	26
4.1 The optical transmission of perovskite films .....	26
4.1.1 two-step deposition method .....	26
4.1.2 two-step deposition method with perovskite seeds.....	29
4.2 The morphology of perovskite films.....	29



4.2.1 two-step deposition method .....	29
4.2.2 two-step deposition method with perovskite seeds.....	31
4.3 The performance of triple-cation perovskite solar cells.....	32
4.3.1 Two-step deposition method.....	32
4.3.2 Two-step deposition method with perovskite seeds .....	35
4.3.3 The comparison of devices from all method.....	40
Chapter V The conclusions .....	44
REFERENCES .....	47
Appendix.....	50
VITA .....	57



## LIST OF TABLES

	<b>Page</b>
Table 1 The band gap of $\text{Cs}_{0.03}(\text{FA}_x\text{MA}_{1-x})_{0.97}\text{PbI}_3$ perovskite films with varied cation ratio. ....	28
Table 2 The band gap of $\text{Cs}_{0.03}(\text{FA}_x\text{MA}_{1-x})_{0.97}\text{Pb}(\text{I}_{0.90}\text{Br}_{0.10})_3$ perovskite films with varied cation ratio. ....	28
Table 3 The best PCEs of $\text{Cs}_{0.03}(\text{FA}_x\text{MA}_{1-x})_{0.97}\text{PbI}_3$ perovskite devices with different cation ratio.	32
Table 4 The best PCEs of $\text{Cs}_{0.03}(\text{FA}_x\text{MA}_{1-x})_{0.97}\text{Pb}(\text{I}_{0.90}\text{Br}_{0.10})_3$ perovskite devices with different cation ratio.....	32



## LIST OF FIGURES

	<b>Page</b>
Figure 1 The PCEs from each kind of solar cells in each year [1] .....	1
Figure 2 Schematics of the normal and inverted structures of a perovskite solar cell [2]. .....	2
Figure 3 The structure of a unit cell of perovskite .....	3
Figure 4 The J-V curves of $\text{FAPbI}_3$ (black), $\text{FA}_{0.85}\text{Cs}_{0.15}\text{PbI}_3$ (red), $\text{FA}_{0.70}\text{Cs}_{0.30}\text{PbI}_3$ (green), and $\text{FA}_{0.55}\text{Cs}_{0.45}\text{PbI}_3$ (orange) [11]. .....	4
Figure 5 The PCEs of triple-cation perovskite solar cell (red circles) and double-cation perovskite solar cell (black squares) at room temperature under full illumination and maximum power point tracking [10]. .....	5
Figure 6 The calculated Goldschmidt tolerance factor of different cations (A) in $\text{APbI}_3$ structure [14]. .....	7
Figure 7 One-step deposition method. ....	9
Figure 8 Two-step deposition method. ....	9
Figure 9 Diagram of optical transmission in a semiconductor. ....	9
Figure 10 The band energy of p-doped (left) and n-doped (right) semiconductors. ....	11
Figure 11 The p-n junction (left) and the band diagram p-n junction (right). ....	12
Figure 12 The band diagram of p-n junction with shifted Fermi levels. ....	13
Figure 13 Energy diagram of perovskite solar cells representing the energy level of each layer [17]. .....	13
Figure 14 Diagram of (left) planar (right) mesoscopic of normal structure of perovskite solar cells [19]. .....	14
Figure 15 The J-V curve of solar cells. ....	16

Figure 16 The J-V curve of solar cell where the light orange box represents the maximum product of current density and voltage and dark orange represents the product of $J_{SC}$ and $V_{OC}$ . .....	17
Figure 17 Schematic showing top view of (a) FTO-coated glass covered by polyimide tape (b) zinc-powder on the uncovered area and applied hydrochloric acid (HCl) (c) finished etched-FTO glass.....	19
Figure 18 Diagram of etched-FTO glass with polyimide tape before compact- and mesoporous- $TiO_2$ .....	20
Figure 19 A complete perovskite solar cells.....	22
Figure 20 The optical transmission of i-ZnO film (left) and triple-cation perovskite films (right). .....	23
Figure 21 The plot of $(\alpha h\nu)^2$ and $h\nu$ of perovskite films. ....	24
Figure 22 The linear line of $(\alpha h\nu)^2$ vs energy from the selected data with the linear equation. .	24
Figure 23 The optical transmission of triple-cation perovskite films (a) $Cs_{0.03}(FA_xMA_{1-x})_{0.97}PbI_3$ and (b) $Cs_{0.03}(FA_xMA_{1-x})_{0.97}Pb(I_{0.90}Br_{0.10})_3$ with different cation ratio. ....	27
Figure 24 The relation between $(\alpha h\nu)^2$ and $h\nu$ where the intercept of x-axis is the optical band gap of perovskite films (a) $Cs_{0.03}(FA_xMA_{1-x})_{0.97}PbI_3$ and (b) $Cs_{0.03}(FA_xMA_{1-x})_{0.97}Pb(I_{0.90}Br_{0.10})_3$ . ....	28
Figure 25 The optical transmission (left) and the plot of $(\alpha h\nu)^2$ and $h\nu$ of perovskite films deposited by two-step deposition method with different seeding concentration (right). ....	29
Figure 26 The SEM images of $Cs_{0.03}(FA_xMA_{1-x})_{0.97}PbI_3$ perovskite films with FA: MA cation ratio (a) 90%: 10%, (b) 85%:15%, (c) 70%:30%, (d) 30:70%, (e) 15%:85%, and (f) 10%: 90% deposited by two-step deposition method. ....	30
Figure 27 The SEM images of $Cs_{0.03}(FA_xMA_{1-x})_{0.97}Pb(I_{0.90}Br_{0.10})_3$ perovskite films with the FA: MA cation ratio (a) 90%: 10%, (b) 85%:15%, (c) 70%:30%, (d) 30:70%, (e) 15%:85%, and (f) 10%: 90% deposited by two-step deposition method. ....	31
Figure 28 SEM images of perovskite films fabricated by two-step deposition method with seeding concentration (a) 7% v/v, (b) 14% v/v, and (c) 20% v/v. ....	31

- Figure 29 J-V curves of (a)  $Cs_{0.03}(FA_xMA_{1-x})_{0.97}PbI_3$  and (b)  $Cs_{0.03}(FA_xMA_{1-x})_{0.97}Pb(I_{0.90}Br_{0.10})_3$  devices. The amount of anti-solvent is 50  $\mu$ l and the active area is 0.06  $cm^2$ . .....33
- Figure 30 The J-V curves of FAPbI<sub>3</sub>-based devices from the conventional method where the cation ratio of FA: MA = 90%: 10% (black line) and 85%: 15% (red line) and the two-step deposition method with perovskite seeding concentration of 7 (blue line), 14 (green line), and 20 (purple line) % v/v. The amount of anti-solvent is 50  $\mu$ l and the active area is 0.06  $cm^2$  .....36
- Figure 31 Box chart plots of solar cell parameters: (a) PCE, (b) FF, (c)  $J_{SC}$ , (d)  $V_{OC}$ , (e)  $R_{shunt}$ , and (f)  $R_{series}$  of FAPbI<sub>3</sub>-based perovskite solar cells fabricated by two-step deposition method with Br-content where cation ratio of FA: MA = 90%: 10% and 85%: 15% and two-step deposition method with perovskite seeds with different seeding concentration. The amount of anti-solvent is 50  $\mu$ l and the active area is 0.06  $cm^2$  .....37
- Figure 32 Box chart plots of parameters: (a) PCE, (b) FF, (c)  $J_{SC}$ , (d)  $V_{OC}$ , (e)  $R_{shunt}$ , and (f)  $R_{series}$  of devices fabricated from two-step deposition with seeding concentration of 7 (blue), 14 (green), and 20 (orange) %v/v. The first row is seeding concentration and the second row is the amount of chlorobenzene (CB). The active area is 0.06  $cm^2$ . .....38
- Figure 33 Cross-section image of a device fabricated by two-step deposition method with seeding concentration 7% v/v and chlorobenzene anti-solvent of 30  $\mu$ l.....39
- Figure 34 The J-V curves of MAPbI<sub>3</sub> devices (purple),  $Cs_{0.03}(FA_xMA_{1-x})_{0.97}Pb(I_{0.90}Br_{0.10})_3$  solar cells fabricated by two-step deposition method with the FA: MA ratio = 90%: 10% (dark green), 85%:15% (light green), 15%: 85% (dark blue), and 10%: 90% (light blue) using 50  $\mu$ l of chlorobenzene and two-step deposition method with seeding concentration 7% (red), 14% (orange), and 20% (yellow) v/v and using 30  $\mu$ l of chlorobenzene. The active area is 0.06  $cm^2$ ...42
- Figure 35 Box chart plots of the parameters: (a) PCE, (b) FF, (c)  $J_{SC}$ , (d)  $V_{OC}$ , (e)  $R_{shunt}$ , and (f)  $R_{series}$  of MAPbI<sub>3</sub> devices (purple),  $Cs_{0.03}(FA_xMA_{1-x})_{0.97}Pb(I_{0.90}Br_{0.10})_3$  solar cells fabricated by two-step deposition method with the FA: MA ratio = 90%: 10% (dark green), 85%:15% (light green), 15%: 85% (dark blue), and 10%: 90% (light blue) using 50  $\mu$ l of chlorobenzene and two-step deposition method with seeding concentration 7% (red), 14% (orange), and 20% (yellow) v/v and using 30  $\mu$ l of chlorobenzene. The active area is 0.06  $cm^2$  .....43

Figure 36 The plot of $(\alpha h\nu)^2$ vs energy of $\text{Cs}_{0.03}(\text{FA}_{0.9}\text{MA}_{0.1})_{0.97}\text{PbI}_3$ with linear equation. ....	50
Figure 37 The plot of $(\alpha h\nu)^2$ vs energy of $\text{Cs}_{0.03}(\text{FA}_{0.85}\text{MA}_{0.15})_{0.97}\text{PbI}_3$ with linear equation. ....	50
Figure 38 The plot of $(\alpha h\nu)^2$ vs energy of $\text{Cs}_{0.03}(\text{FA}_{0.7}\text{MA}_{0.3})_{0.97}\text{PbI}_3$ with linear equation. ....	50
Figure 39 The plot of $(\alpha h\nu)^2$ vs energy of $\text{Cs}_{0.03}(\text{FA}_{0.3}\text{MA}_{0.7})_{0.97}\text{PbI}_3$ with linear equation. ....	51
Figure 40 The plot of $(\alpha h\nu)^2$ vs energy of $\text{Cs}_{0.03}(\text{FA}_{0.15}\text{MA}_{0.85})_{0.97}\text{PbI}_3$ with linear equation. ....	51
Figure 41 The plot of $(\alpha h\nu)^2$ vs energy of $\text{Cs}_{0.03}(\text{FA}_{0.1}\text{MA}_{0.9})_{0.97}\text{PbI}_3$ with linear equation. ....	51
Figure 42 The plot of $(\alpha h\nu)^2$ vs energy of $\text{Cs}_{0.03}(\text{FA}_{0.9}\text{MA}_{0.1})_{0.97}\text{Pb}(\text{I}_{0.9}\text{Br}_{0.1})_3$ with linear equation. .....	52
Figure 43 The plot of $(\alpha h\nu)^2$ vs energy of $\text{Cs}_{0.03}(\text{FA}_{0.85}\text{MA}_{0.15})_{0.97}\text{Pb}(\text{I}_{0.9}\text{Br}_{0.1})_3$ with linear equation. ....	52
Figure 44 The plot of $(\alpha h\nu)^2$ vs energy of $\text{Cs}_{0.03}(\text{FA}_{0.7}\text{MA}_{0.3})_{0.97}\text{Pb}(\text{I}_{0.9}\text{Br}_{0.1})_3$ with linear equation. .....	52
Figure 45 The plot of $(\alpha h\nu)^2$ vs energy of $\text{Cs}_{0.03}(\text{FA}_{0.3}\text{MA}_{0.7})_{0.97}\text{Pb}(\text{I}_{0.9}\text{Br}_{0.1})_3$ with linear equation. .....	53
Figure 46 The plot of $(\alpha h\nu)^2$ vs energy of $\text{Cs}_{0.03}(\text{FA}_{0.15}\text{MA}_{0.85})_{0.97}\text{Pb}(\text{I}_{0.9}\text{Br}_{0.1})_3$ with linear equation. .....	53
Figure 47 The plot of $(\alpha h\nu)^2$ vs energy of $\text{Cs}_{0.03}(\text{FA}_{0.1}\text{MA}_{0.9})_{0.97}\text{Pb}(\text{I}_{0.9}\text{Br}_{0.1})_3$ with linear equation. .....	53
Figure 48 The plot of $(\alpha h\nu)^2$ vs energy of the perovskite sample fabricated by two-step deposition method with 7% v/v perovskite seeding concentration. ....	54
Figure 49 The plot of $(\alpha h\nu)^2$ vs energy of the perovskite sample fabricated by two-step deposition method with 14% v/v perovskite seeding concentration. ....	54
Figure 50 The plot of $(\alpha h\nu)^2$ vs energy of the perovskite sample fabricated by two-step deposition method with 20% v/v perovskite seeding concentration. ....	54

- Figure 51 The optical transmission of triple-cation perovskite films fabricated by two-step deposition method with perovskite seeds. The amount of chlorobenzene is (a) 30 (b) 50 (c) 100  $\mu\text{l}$ . .....55
- Figure 52 SEM images of perovskite films fabricated by two-step deposition method with seeding concentration 7% v/v. The amount of chlorobenzene is (a) 30 (b) 50 (c) 100  $\mu\text{l}$ . .....55
- Figure 53 SEM images of perovskite films fabricated by two-step deposition method with seeding concentration 14% v/v. The amount of chlorobenzene is (a) 30 (b) 50 (c) 100  $\mu\text{l}$ . .....56
- Figure 54 SEM images of perovskite films fabricated by two-step deposition method with seeding concentration 20% v/v. The amount of chlorobenzene is (a) 30 (b) 50 (c) 100  $\mu\text{l}$ . .....56



# Chapter I

## Introduction

### 1.1 Overview

Nowadays, population growth and economic expansion lead to more demand of electricity causing the excessive use of oil, natural gas, etc. Accordingly, these resources will soon be running out and the alternative sources are needed. Sunlight is a renewable energy source and can be used to generate electricity through a solar cell in which a device that converts light energy into electricity by means of photovoltaic effect. Many kinds of solar cells have been invented and one of the fastest developing innovations is a perovskite solar cell where its power conversion efficiency (PCE) continues to grow dramatically, especially during the past decade. At present, the PCE of perovskite solar cells reaches 25.5% as shown in figure 1.

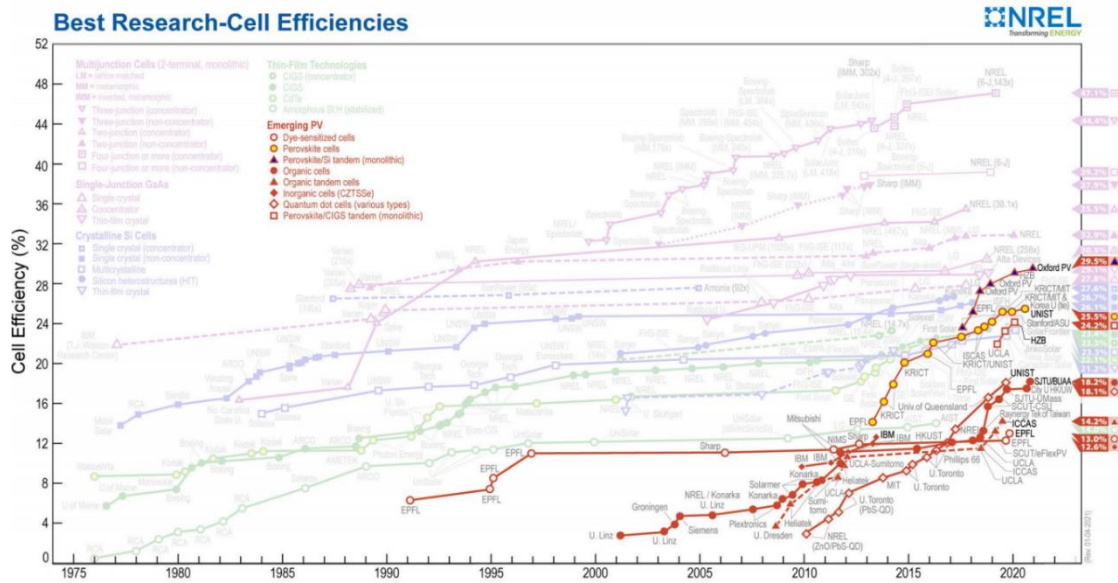


Figure 1 The PCEs from each kind of solar cells in each year [1]

Figure 2 shows that a perovskite solar cell can be categorized into two groups – normal structure (n-i-p structure) and inverted structure (p-i-n structure), the only difference of these structures is the alternating positions of electron transport layer and hole transport layer. In this work, the solar cell structure is the normal structure which typically consists of 5 layers:

- Front contact – fluorine-doped tin oxide-coated (FTO) glass – is used to collect electrons.
- Electron transport layers (ETLs) or blocking layers – compact-TiO<sub>2</sub> and mesoporous-TiO<sub>2</sub> – are used to block holes from an absorber layer to recombine with electrons.



- Absorber layer (photoactive layer) – *perovskite materials* – is the most important layer because it generates carriers, electrons and holes, to produce the current in solar cells.
- Hole transport layer (HTL) – *Spiro-MeOTAD* – is used to improved hole transport into back contact.
- Back contact – *gold or silver* – is used to collect holes from absorber layer.

The layers of perovskite solar cells are mostly prepared by spin-coating (details are described in chapter III).

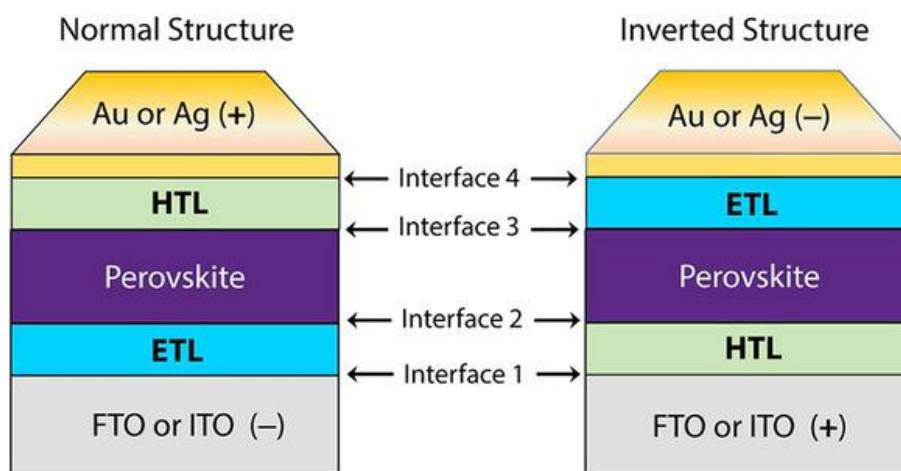


**Figure 2** Schematics of the normal and inverted structures of a perovskite solar cell [2].

### 1.2 A brief history of perovskite

Perovskite was originally named after a Russian mineralogist – Perovski from the discovery of metal oxide  $\text{CaTiO}_3$ . Correspondingly, perovskite or perovskite structure has been interchangeable to describe crystal structure with chemical formula  $\text{ABX}_3$  where A is a cation sitting at the corners of the unit cell, B is a cation at the center of the unit cell, and X is an anion at the face-centered positions of the unit cell as depicted in figure 3. The basic structure of perovskite is a cubic structure with  $\text{BX}_6$  octahedral structure. The perovskite materials for an photoactive layer in solar cells are commonly inorganic-organic cation halide where A is a monovalent cation such as  $\text{CH}_3\text{NH}_3^+$  (methylammonium or MA),  $\text{CH}_3(\text{NH}_2)_2^+$  (formamidinium or FA), and  $\text{Cs}^+$ , B is typically  $\text{Pb}^{2+}$  and X is an halide ion, e.g.,  $\text{I}^-$ ,  $\text{Cl}^-$ , and  $\text{Br}^-$ . The first peer-reviewed paper of perovskite materials for perovskite-based device was  $\text{MAPbI}_3$  and  $\text{MAPbBr}_3$ , and the PCE achieved 3.8 % in 2009 [3]. At times,  $\text{MAPbI}_3$ ,  $\text{MAPbBr}_3$  and  $\text{FAPbI}_3$  can be regarded as *single-cation perovskite materials* since there is only one cation which is “MA” or “FA”.

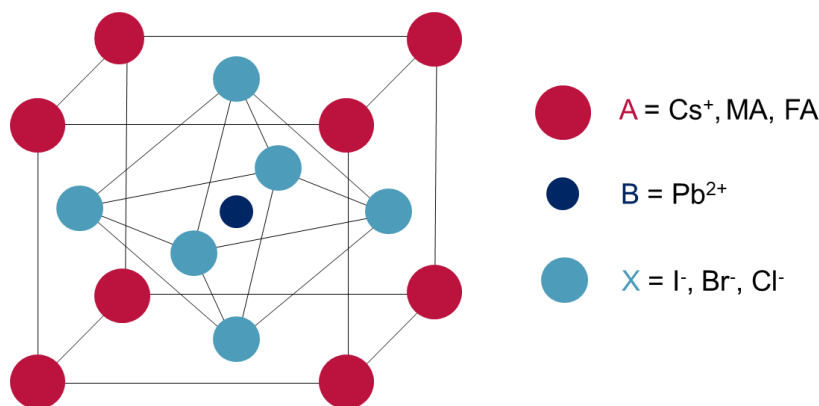


**Figure 3** The structure of a unit cell of perovskite

Earlier, MAPbI<sub>3</sub> has been thoroughly studied and the PCE has succeeded over 20% but the disadvantages of MAPbI<sub>3</sub> are that it is sensitive to heat and humidity [4-6] whereas MAPbBr<sub>3</sub> has too broad band gap (>2 eV) [7]. Another single-cation perovskite that should be mentioned is FAPbI<sub>3</sub> because the band gap of FAPbI<sub>3</sub> is slightly smaller than that of MAPbI<sub>3</sub> including improved charge transport [8], hence the PCE could be enhanced. However, FAPbI<sub>3</sub> lacks structural stability, i.e., two different crystal structures could be attained. One is photo-inactive hexagonal structure or yellow phase and the other one is photo-active perovskite structure or black phase; the names of yellow and black are basically from the color of perovskite samples with such structures. Moreover, the black phase of FAPbI<sub>3</sub> is only stable at 180 °C [9]. As a result, these single-cation perovskite materials seem to have problems especially with the instability. The compositional engineering of perovskite materials is of interest to surpass these problems.

For example, the incorporation of bromide in perovskite material MAPb(I<sub>1-x</sub>Br<sub>x</sub>)<sub>3</sub> (0.06 < x < 0.3) showed the improvement of the devices, the PCE remained the same after exposed to 55% relative humidity for a day while the drop of PCE from MAPbI<sub>3</sub> device was seemingly observed and the color change of MAPbI<sub>3</sub> film from dark brown to yellow was noticed after such condition [5]. *Double-cation* (and mixed halides) *perovskite* solar cells using MA<sub>0.17</sub>FA<sub>0.83</sub>Pb(I<sub>0.83</sub>Br<sub>1.7</sub>)<sub>3</sub> reached the PCE of over 18%. It is because a small amount of MA is sufficient to promote the black phase of FAPbI<sub>3</sub>. In other words, MA acts as a stabilizer of the photo-active structure of FAPbI<sub>3</sub> [10]. The yellow phase yet exists even the device with high PCE. Another double-cation perovskite that was studied is Cs-doped FAPbI<sub>3</sub> and the result showed that the FAPbI<sub>3</sub> device with Cs-doped had better photovoltaic performance than FAPbI<sub>3</sub>

device without Cs as shown in figure 4 [11]. It is worth noting that Cs should not be used more than 15 mol.% because of the phase segregation [12].

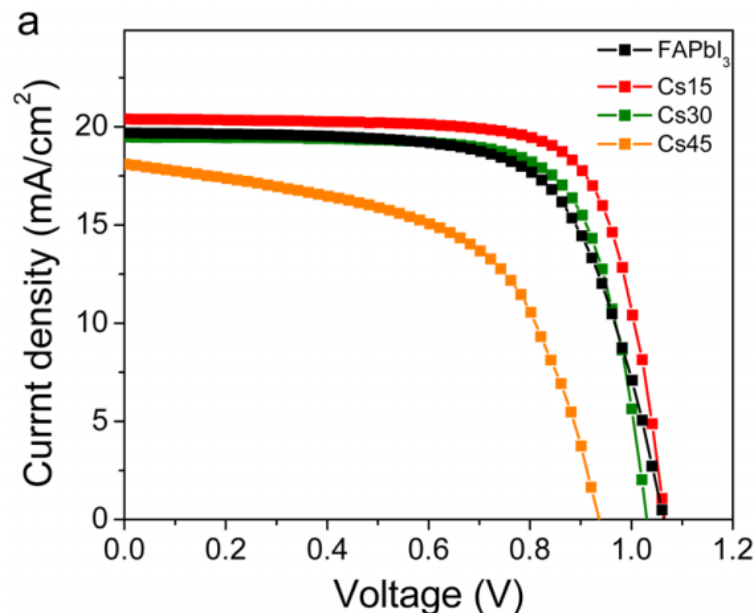


**Figure 4** The J-V curves of FAPbI<sub>3</sub> (black), FA<sub>0.85</sub>Cs<sub>0.15</sub>PbI<sub>3</sub> (red), FA<sub>0.70</sub>Cs<sub>0.30</sub>PbI<sub>3</sub> (green), and FA<sub>0.55</sub>Cs<sub>0.45</sub>PbI<sub>3</sub> (orange) [11].

### 1.3 Triple-cation perovskite solar cells

The mixture of MA, FA, and Cs appears to be a perfect fit to enhance PCE and this kind of perovskite is known as *triple-cation perovskite*. Triple-cation perovskite solar cells, especially FAPbI<sub>3</sub>-based solar cells, has shown excellent performance and stability. For example, Cs<sub>0.1</sub>(FA<sub>0.87</sub>MA<sub>0.13</sub>)<sub>0.9</sub>Pb(I<sub>0.87</sub>Br<sub>0.13</sub>)<sub>3</sub> and FA<sub>0.87</sub>MA<sub>0.13</sub>Pb(I<sub>0.87</sub>Br<sub>0.13</sub>)<sub>3</sub> samples were heated at 130 °C for 3 hours to observe the film color and the results showed that the triple-cation perovskite color retained noticeably dark while the double-cation perovskite color was evidently bleached. Triple-cation perovskite materials demonstrated not only better thermal stability but also structural stability of FAPbI<sub>3</sub>. The XRD data showed that there was a small trace of yellow phase of FAPbI<sub>3</sub> left from double-cation perovskite sample while there was none for triple-cation perovskite sample. In addition, the PCE of 20% was obtained from triple-cation perovskite devices and slightly decreased to 18% which remained stable over 250 hours at room temperature and full maximum power point tracking under full illumination as shown in figure 5 [10].

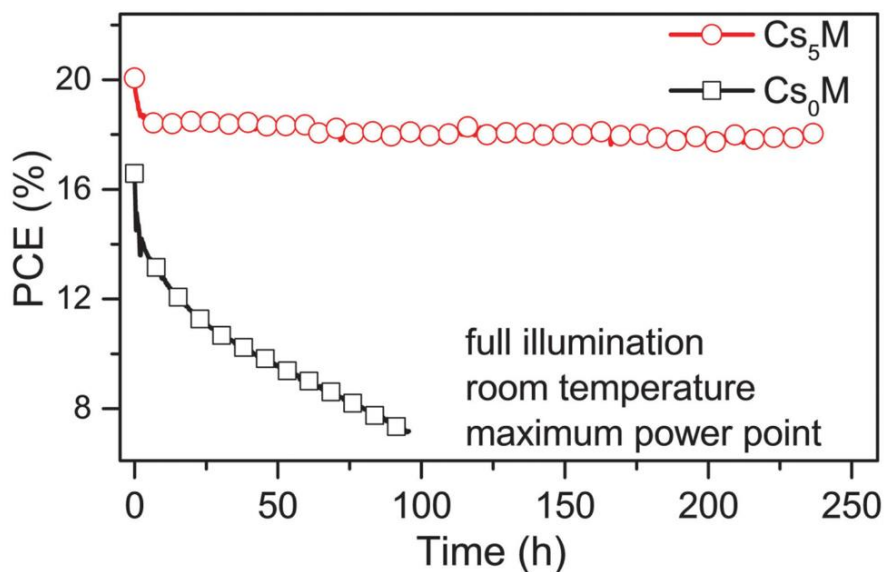


**Figure 5** The PCEs of triple-cation perovskite solar cell (red circles) and double-cation perovskite solar cell (black squares) at room temperature under full illumination and maximum power point tracking [10].

From all of the above, triple-cation perovskite solar cells look promising to examine. In this work, the triple-cation perovskite solar cells were fabricated by two-step deposition method since FAPbI<sub>3</sub>-based triple-cation perovskite devices of two-step deposition method are latterly superior to that of one-step deposition method [13]. The other approach was two-step deposition method with perovskite seeds. The perovskite films were characterized by scanning electron microscopy and optical transmission to obtain the surface morphology and the band gap, respectively. The photovoltaic performance of perovskite solar cells was investigated through J-V characteristics.

#### 1.4 Objectives

- To find appropriate fabrication process and conditions for triple-cation perovskite solar cells.
- To characterize physical and photovoltaic properties of triple-cation perovskite solar cells.
- To compare the performance of triple-cation perovskite solar cells with single-cation perovskite solar cells.

### 1.5 Thesis outlines

In this thesis, it comprises five chapters. Chapter II will mainly be the theory of perovskite structure, band gap of a semiconductor, P-N junction, and solar cell parameters. The experimental procedures and characterization of triple-cation perovskite solar cells will be described in chapter III. The results of the experiments will be demonstrated in chapter IV and the conclusions of the thesis will be in chapter V.



## Chapter II

### Basics of semiconductor, solar cells, and perovskite solar cells

In this chapter, the perovskite structure in terms of Goldschmidt tolerance factor and the concept of perovskite fabrication will be briefly described. Then, the band gap of a semiconductor and P-N junction will be explained. Afterwards, materials of each layer for perovskite solar cells and photovoltaic parameters for the performance of devices will be described.

#### 2.1 Perovskite structure

Goldschmidt tolerance factor generally is an empirical index used to predict the structure of oxide perovskite. Though perovskite materials for solar cells are organic-inorganic halide, the tendency of the structure is still practical [11]. Goldschmidt tolerance factor ( $t$ ) can be expressed as following

$$t = \frac{r_A + r_X}{\sqrt{2}(r_{Pb} + r_X)} \quad (2.1)$$

where  $r_A$  is the radius of A cation,  $r_{Pb}$  is the radius of  $Pb^{2+}$  and  $r_X$  is the radius of halide ion. The perovskite materials tend to form a hexagonal structure when  $t > 1$ , cubic structure when  $0.8 < t < 1$ , and orthorhombic structure when  $t < 0.8$ . A perovskite material may be observed with more than one structure depending on the temperature, for instance, the tolerance factor of  $CsPbI_3$  is lying between cubic and orthorhombic structures. Hence, the structures could be arranged for a cubic structure (black phase) or an orthorhombic structure (yellow phase).

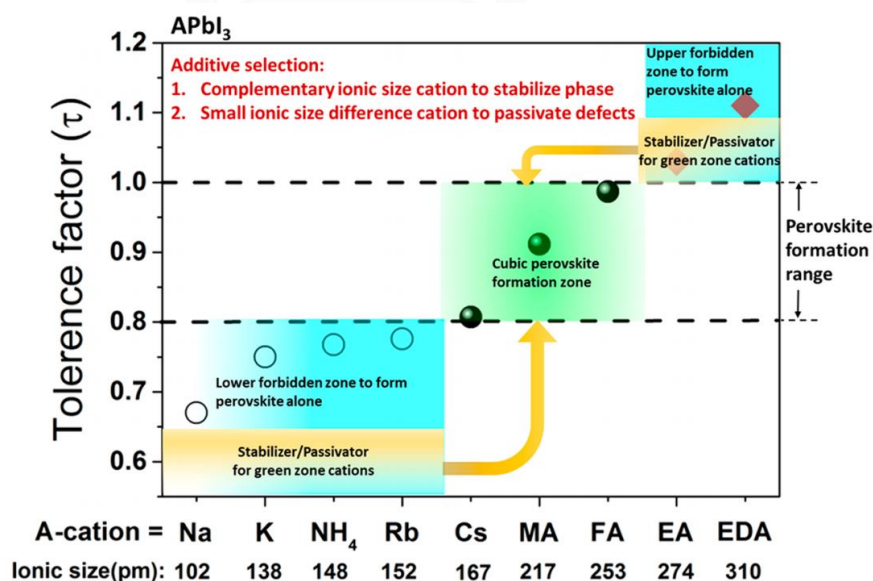


Figure 6 The calculated Goldschmidt tolerance factor of different cations (A) in  $APbI_3$  structure [14].

From figure 6, the estimated ionic radii of FA, MA, and Cs are 2.53, 2.17, and 1.67 Å, respectively. Then, the calculated Goldschmidt tolerance factor of FAPbI<sub>3</sub> is almost 1.0 which means that the predicted structure would be either cubic or hexagonal structure since the value of  $t$  is in-between two structures. The smaller cation, such as MA and Cs, could reduce the Goldschmidt factor of FAPbI<sub>3</sub> and gain the cubic structure. This concurs what mentioned earlier in chapter I that the black phase (or cubic structure) of FAPbI<sub>3</sub> could be stabilized by MA and Cs. Nonetheless, these Goldschmidt factors are not totally the answer to determine the exact structures of perovskite materials particularly organic-inorganic halide because it is difficult to calculate the exact radius of organic ion [8]. According to figure 6, the  $t$  value of MAPbI<sub>3</sub> is 0.9 and the structure should be cubic. Instead, the structure of MAPbI<sub>3</sub> is experimentally tetragonal with a tilting of PbI<sub>6</sub> octahedra where the  $t$  value is 0.9 and the structure of the black phase FAPbI<sub>3</sub> is trigonal (some would call this structure pseudo-cubic structure because it is closed to a cubic structure). At this point, it was found that the perovskite structure is accounted to the interplay of the cation size and the hydrogen bonds between FA/MA cations and the inorganic matrix of I [8] because a higher probability of FA to form hydrogen bonds comparing to MA induces the stabilization of the pseudo-cubic structure. Additionally, the difference of crystal structures could affect the electronic and optical properties of perovskite materials. For example, the pseudo-cubic structure of FAPbI<sub>3</sub> enhances spin-orbit coupling effect due to the increased ionic character of Pb. This causes the red shift of the onset absorption of perovskite materials and improved charge transport [8] compared to the tetragonal structure of MAPbI<sub>3</sub>.

## 2.2 Perovskite fabrication

The approaches to fabricate triple-cation perovskite films are roughly classified into two major categories: solution-based deposition methods and vapor-based deposition methods. In this work, the first method will be employed since the latter requires costly tools. The solution-based deposition method is related to spin-coating. It is a technique in which the solution is firstly dropped onto the substrate and then the substrate is rotated at some speed to spread out the solution covering the surface by the centrifugal force. Generally, there are roughly two kinds of spin-coating to deposit perovskite layers which are one-step deposition method and two-step (or sequential) deposition method. Figure 7 demonstrates one-step deposition method, which is a process that all perovskite materials are mixed in the solvent, then spin-coated on the substrate

and the substrate is annealed to eliminate excessive solvent and assist the forming of perovskite crystallite, while two-step deposition process is a process in which lead-halide precursor is firstly spin-coated then organic cation solution is deposited onto lead-halide layer as illustrated in figure 8. In this research, the two-step deposition method was chosen to fabricate the layer.

### Perovskite Solution

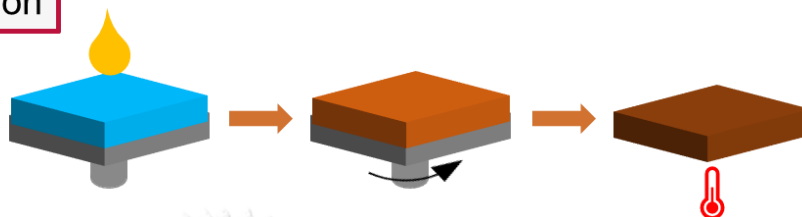


*Figure 7 One-step deposition method.*

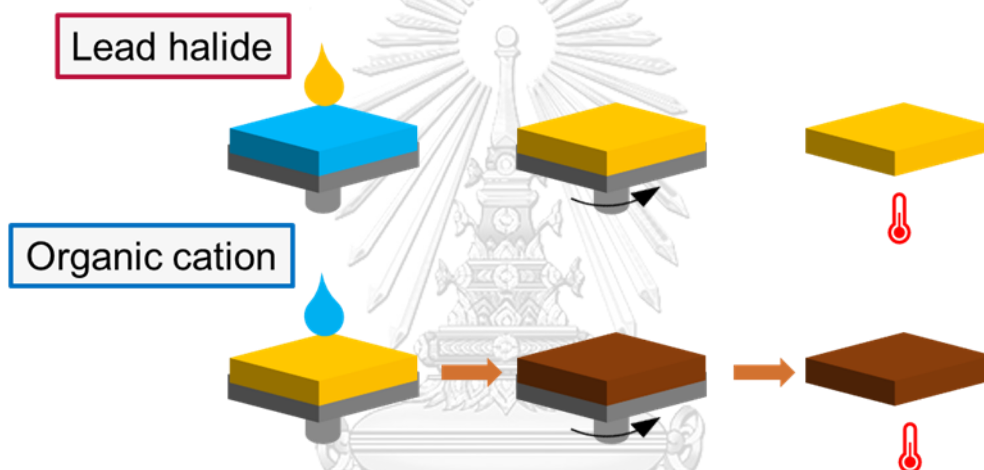


*Figure 8 Two-step deposition method.*

### 2.3 Band gap energy

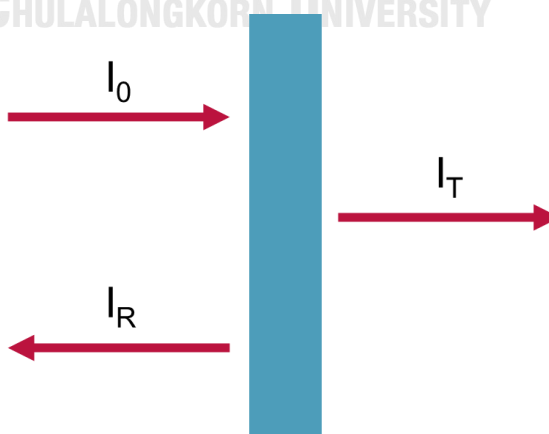


*Figure 9 Diagram of optical transmission in a semiconductor.*



When the light of which intensity is  $I_0$  perpendicularly falls onto a semiconductor (figure 9), the intensity of light decreases as light travels through a semiconductor due to the absorption of a semiconductor. For convenience, the absorption can be used as absorption coefficient which can be written as following

$$\alpha = -\frac{1}{I(x)} \frac{dI(x)}{dx}, \quad (2.2)$$

where  $I(x)$  is the intensity of light at the distance  $x$  in a semiconductor,

$x$  is the distance of light through a semiconductor,

$\alpha$  is the absorption coefficient.

The minus sign in equation (2.2) suggests the intensity of light decreases as the light gets through the substance. From equation (2.2), if the incident light is  $I_0$  at  $x = 0$ , thus the intensity at any given distance in a semiconductor is

$$I(x) = I_0 e^{-\alpha x}. \quad (2.3)$$

Transmittance ( $T$ ) and reflectance ( $R$ ) can be written in terms of incident light ( $I_0$ ), transmitted light ( $I_T$ ), and reflected light ( $I_R$ ) as following

$$T = \frac{I_T}{I_0}, \quad (2.4)$$

$$R = \frac{I_R}{I_0}. \quad (2.5)$$

Typically, the transmittance could be used as percent transmission ( $\%T$ )

$$\%T = \frac{I_T}{I_0} \times 100. \quad (2.6)$$

And from equation (2.3) and (2.6), if the thickness of a semiconductor is  $d$ , the absorption coefficient can be calculated from this equation

$$\alpha = -\frac{1}{d} \ln \left( \frac{\%T}{100} \right), \quad (2.7)$$

where  $\alpha$  is the absorption coefficient,

$\%T$  is percent transmission,

$d$  is the thickness of a semiconductor.

For absorption process in semiconductors, a photon can be absorbed by a semiconductor when the energy of photon is equal or greater than the band gap, an electron from valence band will be excited to conduction band and becomes free electron in the conduction band and hole in the valence band, it is called an electron-hole pair. When an electron in the conduction band falls back to the valence band it is called a recombination. If the momentum of the process is conserved, this semiconductor has a direct band gap. On the other hand, if the momentum of the

process is not conserved, the semiconductor has an indirect band gap. The direct and indirect band gap can be evaluated from the absorption coefficient by using the relation

- Direct band gap

$$\alpha h\nu = A(h\nu - E_g)^{1/2}, \tag{2.8}$$

- Indirect band gap

$$\alpha h\nu = A(h\nu - E_g)^2, \tag{2.9}$$

where  $\alpha$  is the absorption coefficient,

$h$  is Planck's constant =  $6.62 \times 10^{-34}$  m<sup>2</sup>kg/s,

$\nu$  is a frequency of photon,

$A$  is a constant,

$E_g$  is the band gap.

Since most materials have direct band gap including perovskite, the equation (2.8) is applied by using Tauc plot of  $(\alpha h\nu)^2$  vs.  $h\nu$  and the band gap can be estimated from the intercept of the extrapolation of a straight line on  $h\nu$  axis [15].

### 2.4 P-N junction

Consider p-doped and n-doped semiconductors. A p-doped semiconductor contains positively charged holes while an n-doped semiconductor has negatively charged electron. Both semiconductors are neutrally charged because the charges of the carriers (electrons and holes) are compensated by charged ions. Fermi level of p-doped semiconductors is closed to the bottom of the valence band and fermi level of n-doped semiconductors is closed to the top of the conduction band as illustrated in figure 10.

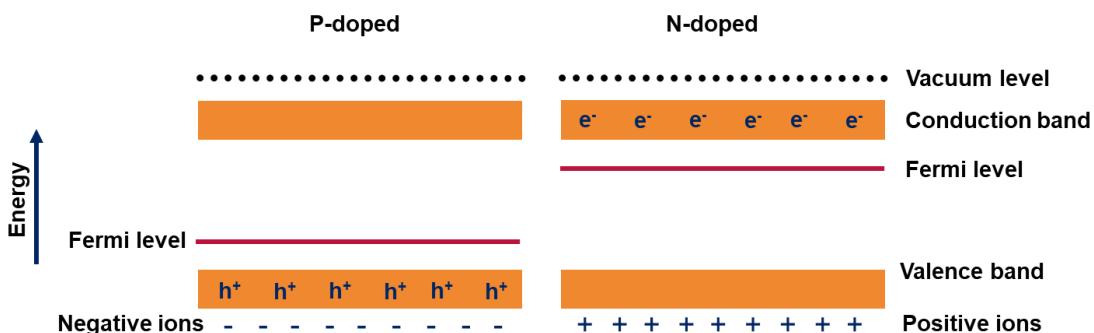


**Figure 10** The band energy of p-doped (left) and n-doped (right) semiconductors.

When n-doped and p-doped semiconductor are made in contact, electrons from n-doped semiconductor (higher Fermi level) will flow into the side of p-doped semiconductor (lower Fermi level) and holes from p-doped semiconductor will flow into the side of n-doped semiconductor. This will result in the depleted of electrons in n-doped semiconductor and the depleted of holes in p-doped semiconductor at the interface, this region is called the depletion region. At the depletion region, the net charge of fixed ions in the n-doped semiconductor is positive whereas the net charge of fixed ions in the p-doped semiconductor is negative. Those fixed charged ions from both semiconductors produce the electric field as illustrated in figure 11 and a built-in potential is created.

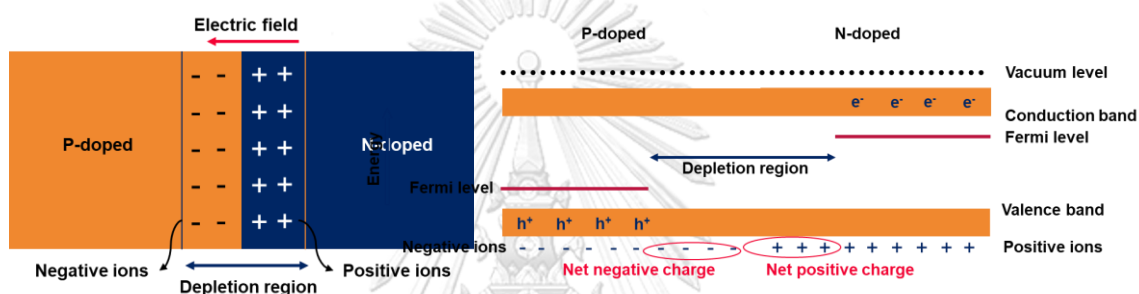


**Figure 11** The p-n junction (left) and the band diagram p-n junction (right).

However, the band diagram of p-n junction from figure 11 on the right-hand side is not completely correct. When electrons flow to p-doped semiconductor and holes flow to n-doped semiconductor until the electric field is large enough, the Fermi levels of both sides should be equal. Figure 12 shows the shifted fermi level of the semiconductors and both semiconductors share the same fermi level. When exposing P-N junction to light, photons are absorbed and electron-hole pairs are created at the depletion region, the electrons will go to the right or lower conduction band and the holes will flow to the left or higher valence band due to electric field at the depletion region. Thus, a net current occurs [16]. Such principle can be applied to perovskite solar cell structure because a solar cell is as well a p-n junction device. Figure 13 exhibits the example of band gap of all layers for perovskite solar cells which should be aligned and conformed the principle. Once photons are absorbed by perovskite layer and electron-hole pairs are created, electrons at the conduction band will flow into the lower conduction band (to the left) and be collected at FTO layer whereas holes at the valence band will flow into the higher valence band (to the right) and be collected at metal contact.

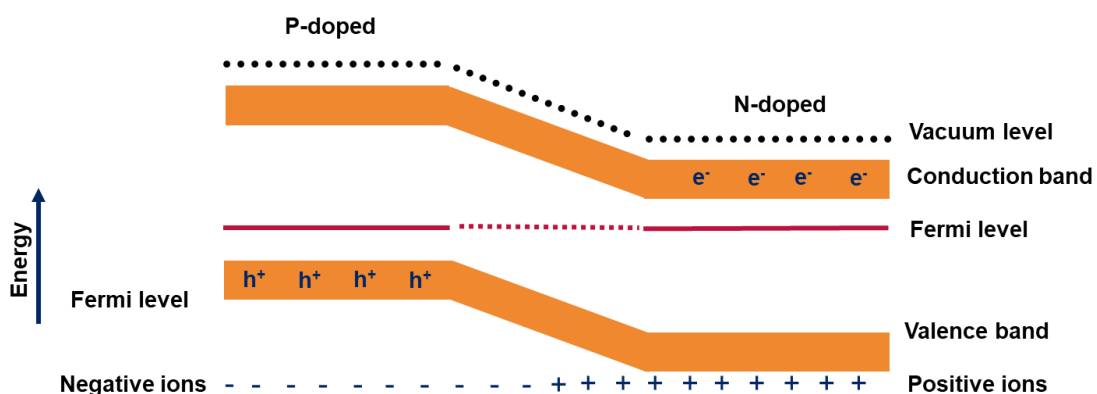


*Figure 12 The band diagram of p-n junction with shifted Fermi levels.*

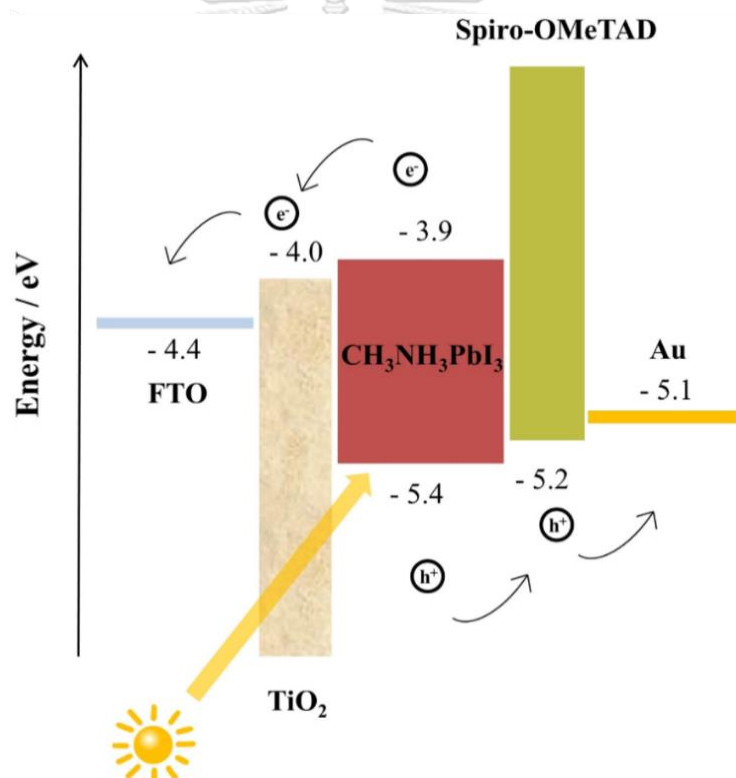


*Figure 13 Energy diagram of perovskite solar cells representing the energy level of each layer*

[17].

## 2.5 Perovskite solar cell structure

From the notion of the last section, band gap of each layer should be aligned as in figure 13 but the desire for each layer is more than that. In this part, the details of each layer will be revealed.

### 2.5.1 Front contact

Front contact for perovskite solar cells is used to collect electrons from a photoactive layer. The requirement properties of this layer must be transparent and have excellent conductivity as well as thermal resistance because the fabrication of some following layers might need very high temperature. Fluorine-doped tin oxide (FTO)-coated glasses were selected due to the transparency, relatively stable under atmospheric condition, chemically inert, and high-temperature resistance. ITO or indium tin oxide-glasses could be used as well. However, it is actually more expensive than FTO-glasses.

### 2.5.2 Electron transport layer or blocking layer

This layer must be transparent conducting film and n-type semiconductor because the light must get through to an absorber layer and another function of the layer is to prevent holes to recombine with electrons. Normal structure of perovskite solar cells can be categorized by electron transport layer as demonstrated in figure 14. First is a planar type in which there is only one electron transport layer, e.g., compact-TiO<sub>2</sub> or SnO<sub>2</sub>. The other is mesoscopic type where there is an additional layer which is scaffold mesoporous-TiO<sub>2</sub>, such layer can reduce the hysteresis of devices [18]. Compact-TiO<sub>2</sub> and mesoporous-TiO<sub>2</sub> materials were chosen for this research.

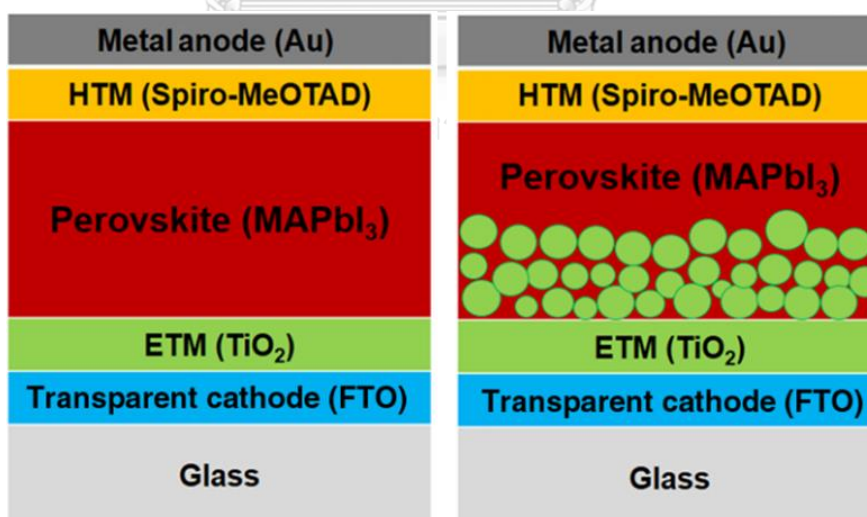


**Figure 14** Diagram of (left) planar (right) mesoscopic of normal structure of perovskite solar cells [19].

### 2.5.3 Photoactive layer

This layer is the most important layer because it generates carriers, electrons and holes, to produce the current from solar cells. The triple-cation perovskite material for an absorber layer will be focused. The triple-cation perovskite films typically has its form of  $(\text{Cs/FA/MA})\text{Pb}(\text{I/Br})_3$  where the amount of FA, and MA were varied in this work.

### 2.5.4 Hole transport layer

Hole transport layer is deposited prior to back contact to avoid the recombination of electrons and holes resulting in increasing fill factor [20]. Many types of hole transport layer have been employed for normal structure of perovskite solar cells, such as, spiro-MeOTAD, CuSCN, and PCBM. Spiro-MeOTAD was selected for the research because of great photovoltaic performance in perovskite devices. Nevertheless, spiro-MeOTAD needs dopant like Li-TFSI so as to improve conductivity and accelerate oxidization [21].

### 2.5.5 Back contact

Gold or silver are commonly used for this layer. Although silver is relatively low-cost compared to gold, silver after exposing to air was corroded and silver iodide was formed when MAI migrated through the small pinholes in spiro-MeOTAD causing poor performance of solar cells [22]. Thus, gold was selected as back contact and fabricated by means of thermal evaporation.

## 2.6 Solar cell parameters

Fundamental photovoltaic parameters of solar cell are power conversion efficiency (PCE), fill factor (FF), short-circuit current density ( $J_{sc}$ ), open-circuit voltage ( $V_{oc}$ ), shunt resistance ( $R_{shunt}$ ), and series resistance ( $R_{series}$ ). Figure 15 shows a J-V curve of a solar cell when it is exposed to light.

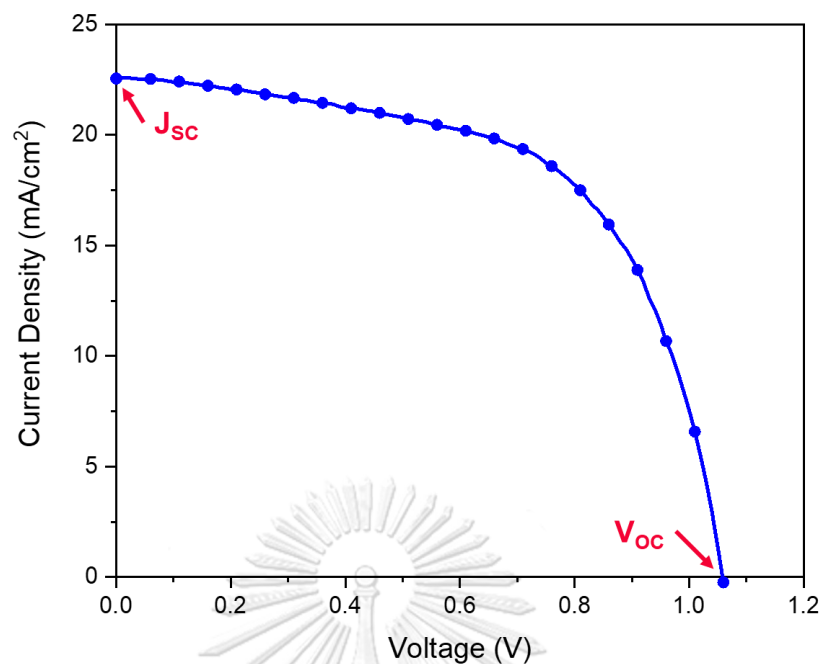


**Figure 15** The  $J$ - $V$  curve of solar cells.

Short-circuit current density is the maximum current density generated by solar cells or the current density when the voltage across the device is zero. The current density is rather used than just the current to avoid the influence of active area because the current firmly depends on the active area of solar cells. Open-circuit voltage is the maximum voltage produced by solar cells or the voltage when the current is zero.

Fill factor is a parameter used to describe how close the ideal of such a solar cell is. Fill factor is defined as the ratio of the maximum product of current density and voltage (the yellow area) to the product of  $J_{sc}$  and  $V_{oc}$  (the orange area) as shown in figure 16 and equation 2.14. Fill factor can be considered a measure of squareness of the  $J$ - $V$  curve. If the curve is squarer, the curve takes more area. The values of FF are in between 0 and 1, when the value closed to 1, it means the solar cell is impeccable (closed to ideal) while the value closed to 0 means the solar cell is poor. Fill factor relies on the shunt resistance and series resistance. Shunt resistance originates from the leakage paths in devices which allows the current to flow other paths. The leakage path in perovskite devices in general arises from the pinholes in photoactive layer and recombination losses. Series resistance is responsible to internal resistance, e.g., perovskite layer, charge-collecting interlayer, and metal electrode [23, 24]. As a matter of fact, shunt resistance should be very large whereas series resistance should be very low to acquire the decent fill factor.

Moreover, short-circuit current density is also affected by both resistances while open-circuit voltage is dependent to only shunt resistance, according to generalized Shockley's equations [25].

$$J_{SC} = J_{Ph} - J_0 \left[ \exp \left( \frac{q(V - JR_S)}{nkT} - 1 \right) \right] - \frac{V - JR_S}{R_{Sh}}, \quad (2.10)$$

$$V_{OC} = \frac{nkT}{q} \ln \left( \frac{J_{Ph}}{J_0} \left[ 1 - \frac{V_{OC}}{J_{Ph} R_{Sh}} \right] \right), \quad (2.11)$$

where  $J_{Ph}$  is photocurrent density,

$J_0$  is reverse bias saturation current density,

$q$  is elementary charge,

$R_S$  is series resistance,

$R_{Sh}$  is shunt resistance,

$n$  is the diode ideality factor,

$T$  is the room temperature.

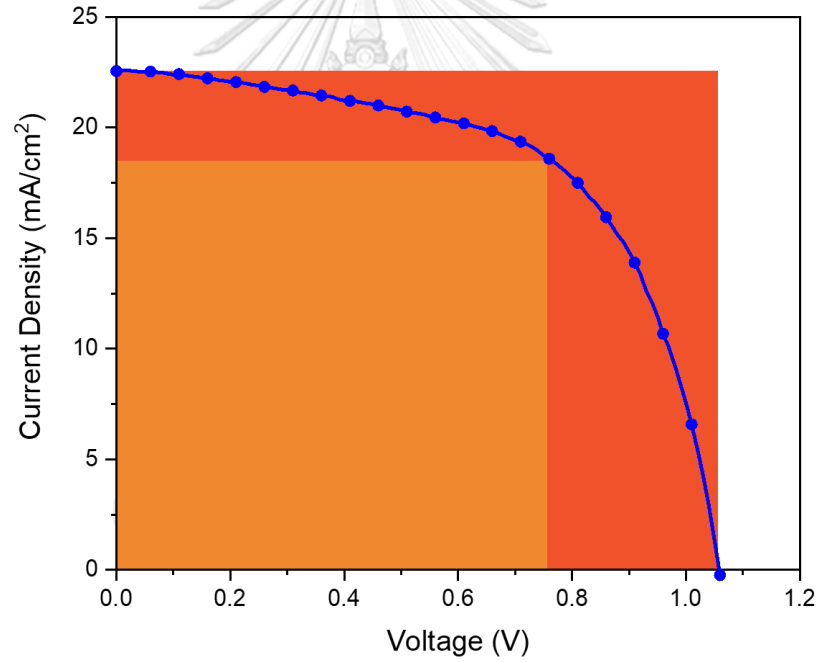


**Figure 16** The J-V curve of solar cell where the light orange box represents the maximum product of current density and voltage and dark orange represents the product of  $J_{SC}$  and  $V_{OC}$ .

Power conversion efficiency (PCE) is defined as the fraction of the maximum power from solar cell to the input power from the light as following equation

$$PCE = \frac{P_{output}}{P_{input}} \times 100. \quad (2.12)$$

And it can be rewritten as



$$PCE = \frac{(J \times V)_{max}}{I} \times 100, \quad (2.13)$$

where  $(J \times V)_{max}$  is the maximum product of current density and voltage,

$I$  is the irradiance (the unit is W/area) and set at  $100 \text{ mW/cm}^2$  which is the sunlight under 1.5 AM condition.

Since  $FF$  is the ratio of the maximum product of current density and voltage to the product of  $J_{sc}$  and  $V_{oc}$

$$FF = \frac{(J \times V)_{max}}{J_{sc} \times V_{oc}}. \quad (2.14)$$

Thus equation (2.13) can be rewritten as

$$PCE = \frac{V_{oc} \times J_{sc} \times FF}{I} \times 100. \quad (2.15)$$

Power conversion efficiency reflects the performance of devices. Form the equation (2.15), the PCE of devices strongly depends on open-circuit voltage, short-circuit current density, and fill factor. However, the limitation is that if  $V_{oc}$  is high, it means that the band gap is large. As a result,  $J_{sc}$  will be reduced due to the broaden absorption range.

## Chapter III

### Fabrication and Characterization

In this chapter, the preparation of the substrates and materials will be briefly described. Then the fabrication processes of triple-cation perovskite solar cells from electron transport layer to back contact will be fully explained, especially the fabrication of triple-cation perovskite layer. And the last section is the characterization of perovskite solar cells.

#### 3.1 Preparation of substrates and materials for perovskite solar cells

##### 3.1.1 Front contact

A 3 mm thick of FTO-coated glass is cut into  $3 \times 3 \text{ cm}^2$  and etched to prevent the short circuit. FTO-coated glass is covered by polyimide tape with  $2 \text{ cm} \times 3 \text{ cm}$  as illustrated in figure 17, then zinc-powder is spread on the top of uncovered area and a couple drops of hydrochloric acid are applied at zinc-powder area to take out or etch the FTO film. After that, the FTO-etched glass is cleaned by using an ultrasonic bath with detergent, DI water, acetone, and 2-propanol, sequentially for 30 minutes each.

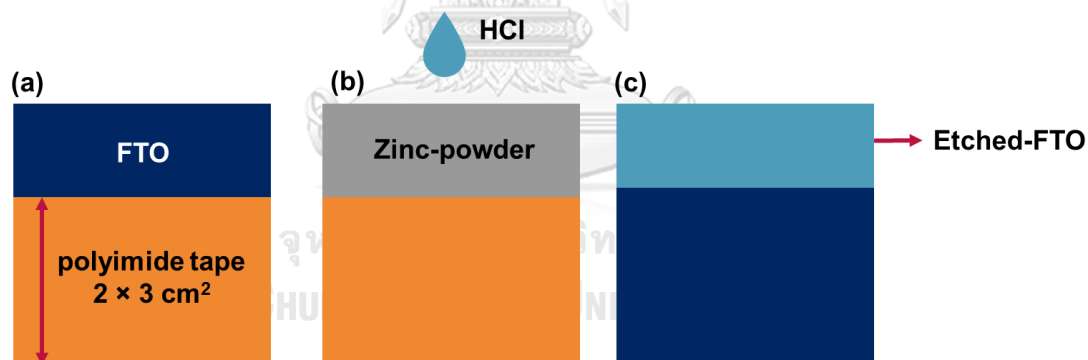


**Figure 17** Schematic showing top view of (a) FTO-coated glass covered by polyimide tape (b) zinc-powder on the uncovered area and applied hydrochloric acid (HCl) (c) finished etched-FTO glass.

##### 3.1.2 Electron transport layer(s)

Commercially available compact-TiO<sub>2</sub> liquid is mixed with ethanol in the volume ratio of 1:2, then stirred overnight at 70 °C. Commercially available mesoporous-TiO<sub>2</sub> liquid is mixed with ethanol in the volume ratio of 1:7, then stirred overnight at room temperature. Before fabrication, the cleaned substrate is taped at the opposite of the etching-side of the glass using

polyimide tape as depicted in figure 18 to avoid short circuit. However, before annealing process, the tape must be removed because the tape can be melted at high temperature.

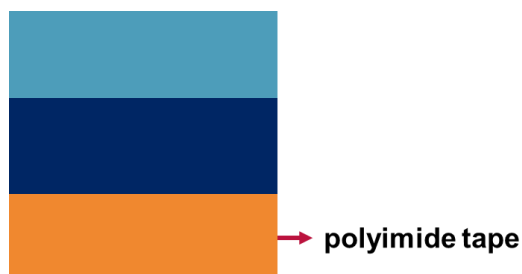


**Figure 18** Diagram of etched-FTO glass with polyimide tape before compact- and mesoporous-

$TiO_2$

### 3.1.3 Absorber layer

#### 3.1.3.1 Two-step deposition method

As previously mentioned in chapter II, two-step deposition method is chosen to study. The content of Cs is fixed at 3% of cations ( $Cs_{0.03}(FA_xMA_{1-x})_{0.97}$ ) and the content of FA and MA cations of atomic percent were varied for the ratio of FA:MA = 90%:10%, 85%: 15%, 70%: 30%, 30%: 70%, 15%: 85%, and 10%: 90%. Moreover, the effect of Br in triple-cation perovskite solar cells is further studied by varying the content of bromide for 0 and 10% of halide ions (I and Br). Therefore, the triple-cation perovskite with 10% Br-contained could be written as  $Cs_{0.03}(FA_xMA_{1-x})_{0.97}Pb(I_{0.9}Br_{0.1})_3$ .

In case of triple-cation perovskite layer without bromide, 1 M of  $PbI_2$  is dissolved in DMF: DMSO = 4:1 volume ratio and stirred overnight at 70 °C. In case of triple-cation perovskite layer with 10% of bromide, 1 M of  $PbI_2$  and 0.14 M of  $PbBr_2$  is dissolved in DMF: DMSO = 4:1 volume ratio and stirred overnight at 70 °C. The total concentration of FAI and MAI is 10 mg/ml by preparing FAI and MAI salts with the ratio 90%:10%, 85%: 15%, 70%: 30%, 30%: 70%, 15%: 85%, and 10%: 90%, then dissolved in IPA (2-propanol) and stirred overnight at room temperature. However, CsI has a low solubility and IPA is a relatively weaker solvent compared to DMF. As a result, CsI cannot dissolve with the organic cation salts in IPA solvent. Thus, 1.5 M of CsI is dissolved in DMF: DMSO = 4:1 volume ratio and stirred overnight at room temperature. Before lead halide fabrication, CsI solution is added into lead halide precursor and kept stirring for 10 minutes.

### 3.1.3.2 Two-step deposition method with perovskite seeds

This method is a modified of two-step deposition method where perovskite seeds is separately prepared and added into lead halide solution. For this method, the concentrations of perovskite seeding precursor in  $\text{PbI}_2$  solution of 7, 14, and 20 %v/v are studied in the work.

1.4 M of  $\text{PbI}_2$  is dissolved in 1 ml DMF and 160  $\mu\text{l}$  DMSO and stirred overnight at 70 °C. The seeding precursor is prepared by 1.2 M of  $\text{PbI}_2$ , 0.21 M of  $\text{PbBr}_2$ , 1.08 M of FAI, 0.18 M of MABr, and 0.14 M of CsI dissolved in DMF: DMSO = 4:1 volume ratio and stirred at 60 °C for 10 minutes to form  $\text{Cs}_{0.09}\text{FA}_{0.77}\text{MA}_{0.14}\text{Pb}(\text{I}_{0.85}\text{Br}_{0.15})_3$  as perovskite seeds, and then the seeding precursor is mixed into  $\text{PbI}_2$  solution and kept stirring at 70°C for 15 minutes. 8.3 mg of FAI, 0.83 g of MABr, and 0.87 mg of MAI are dissolved in 10 ml of IPA and stirred overnight at room temperature.

#### 3.1.4 Hole transport layer

0.0723 g of Spiro-MeOTAD powder is dissolved in 1 ml of chlorobenzene and stirred overnight at room temperature. 28.8  $\mu\text{l}$  of 4-tert-butylpyridine (t-BP) and 17.5  $\mu\text{l}$  of Lithium-bis(trifluoromethanesulfonyl)amide (Li-TFSI) of which 0.52 g dissolved in 1 ml of acetonitrile are mixed in 1 ml of Spiro-MeOTAD and kept stirring for 3 hours before use.

### 3.2 Deposition processes of each layer for perovskite solar cells

Before fabrication, FTO-coated glasses are cleaned with  $\text{UV-O}_3$  for 10 minutes. Then 400  $\mu\text{l}$  of compact- $\text{TiO}_2$  is dropped onto the substrate and spin-coated at 3000 rpm for 30s. After that, the substrate is placed on the hot plate at 500 °C for 30 minutes. Next, 400  $\mu\text{l}$  of mesoporous- $\text{TiO}_2$  is dropped onto the substrate and spin-coated at 3000 rpm for 30s. After that, the substrate is annealed at 500 °C for 30 minutes. The substrates then are cleaned with  $\text{UV-O}_3$  for 10 minutes and preheated at 70 °C to refrain from the temperature difference between substrates and lead halide solution.

For conventional two-step deposition method, 200  $\mu\text{l}$  of lead-halide precursor is spin-coated onto the substrates at 3000 rpm for 30s then annealed at 70 °C for 20 minutes and cool down. After that, 400  $\mu\text{l}$  of organic cation precursor is spin-coated at the rate of 2000 rpm for 20s, and repeated again, then followed by 50  $\mu\text{l}$  of chlorobenzene as anti-solvent after the substrate is spinning for 5s. After this, the substrate is heated at 140 °C for 10 minutes.

For two-step deposition method with perovskite seeds, 150  $\mu\text{l}$  of  $\text{PbI}_2$  solution with seeds is spin-coated onto the substrate at the rate of 3000 rpm for 30s then annealed at 70  $^\circ\text{C}$  for 20 minutes and cool it down. Next, 400  $\mu\text{l}$  of organic cation precursor is deposited at the rate of 2000 rpm for 20s, and repeated again, then followed by 50  $\mu\text{l}$  of chlorobenzene as anti-solvent after the substrate is spinning for 5s. After this, the substrate is heated at 140  $^\circ\text{C}$  for 10 minutes.

150  $\mu\text{l}$  of spiro-MeOTAD is deposited onto perovskite layer by spin-coating at the rate of 3000 rpm for 30s. The sample is left overnight for oxidization of spiro-MeOTAD [21]. All processes are conducted in nitrogen-filled glove box with water content 0.1 ppm and oxygen content lower than 1 ppm. Finally, 120 nm thick of Au is thermally evaporated on the top of spiro-MeOTAD layer.

It is worth noting that the color of perovskite films for solar cells after fabrication process should be dark brown or black at room temperature because the perovskite films naturally absorb the light over visible spectrum and the figure 19 shows the examples of the completed triple-cation perovskite solar cells after thermal evaporation of gold.

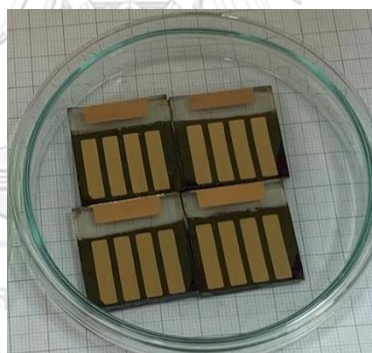


*Figure 19* A complete perovskite solar cells.

### 3.3 Characterization of perovskite solar cells

The perovskite layer is deposited onto the  $\text{FTO}/\text{compact-TiO}_2/\text{mesoporous-TiO}_2$  to investigate the optical transmission and morphology of perovskite films. The optical property and morphology of perovskite films are investigated by optical transmission and scanning electron microscopy, respectively. The photovoltaic performance of perovskite solar cells is characterized via J-V characteristics, under AM1.5 condition.

### 3.3.1 Percent transmission

The optical transmission (%T) of perovskite films was examined by a UV/VIS spectrophotometer (Shimadzu: Model UV-1610PC) in the range of 350 – 1100 nm and used to estimate the optical band gap of triple-cation perovskite films.

### 3.3.2 The calculation of optical band gap

The band gap of a perovskite layer can be obtained from transmission data and the thickness of the perovskite film, according to equation 2.8. For perovskite film, however, it is a bit more complex than usual. Figure 20 demonstrates plots of percent transmission of intrinsic-ZnO layer (on the left) and perovskite MAPbI<sub>3</sub> layer (on the right). The optical transmission of intrinsic-ZnO film completely drops to zero which means the photons are fully absorbed and the equation 2.7 can be simply calculated. While the optical transmission of perovskite film quickly drops at the region 1 and is supposed to drop to zero, but another slope of transmission occurs at the region 2 because of the uncomplete transformation of PbI<sub>2</sub> into MAPbI<sub>3</sub> or FAPbI<sub>3</sub> perovskite. So, in this case, the only data at the region 1 should be selected to estimate the band gap. To determine the band gap, the absorption coefficient should be calculated first.

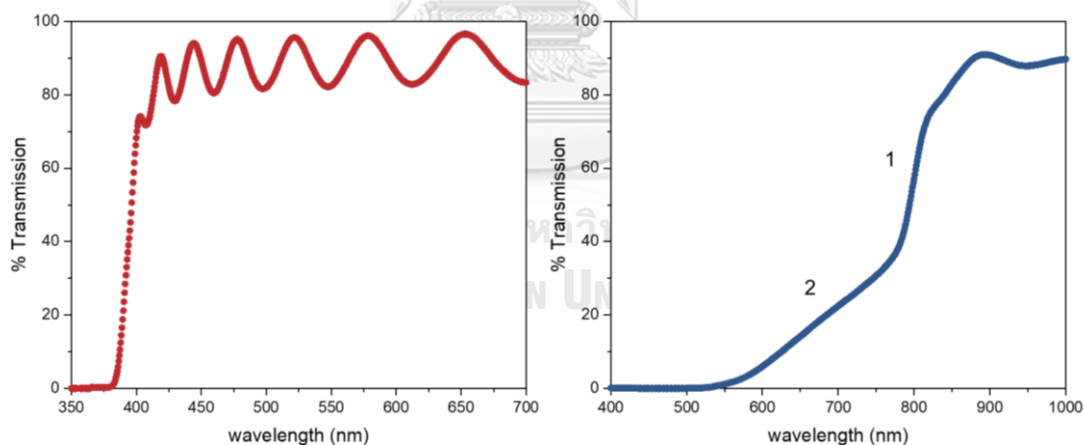


**Figure 20** The optical transmission of *i*-ZnO film (left) and triple-cation perovskite films (right).

The thickness of perovskite layer should be firstly obtained which could be obtained from cross-section SEM image. Secondly, the optical transmission and the thickness of perovskite film are applied in equation 2.7 to attain the absorption coefficient. Next, the calculated absorption coefficient is used by plotting  $(\alpha hv)^2$  as y-axis and  $hv$  as x-axis. Figure 21 shows a graph plotted between  $(\alpha hv)^2$  and  $hv$ . From equation 2.8, the band gap could be acquired from linear relation. Thus, the data in the region 1 is selected to plot and construct linear equation as

shown in figure 22. From the linear equation  $y = mx + c$ , the band gap can be estimated by  $-b/m$ . Therefore, the band gap of the MAPbI<sub>3</sub> perovskite is  $11.55/7.211 = 1.60$  eV.

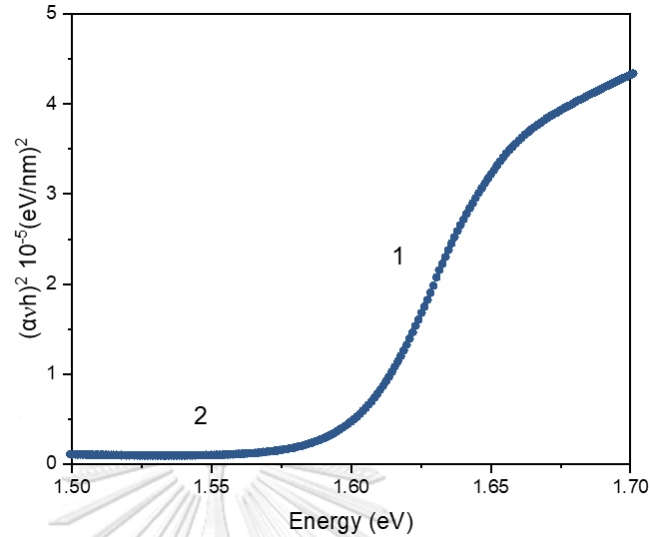


**Figure 21** The plot of  $(\alpha h\nu)^2$  and  $h\nu$  of perovskite films.

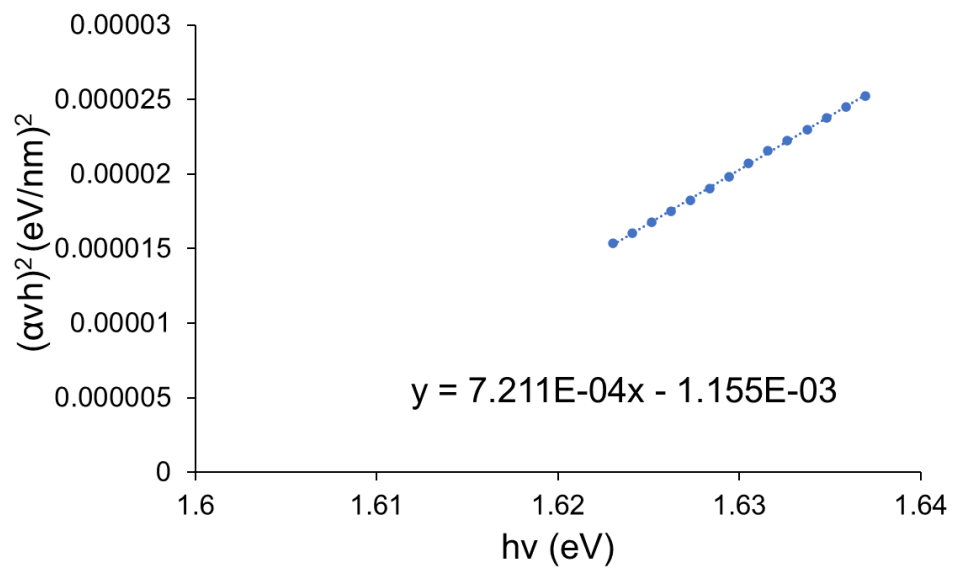


**Figure 22** The linear line of  $(\alpha h\nu)^2$  vs energy from the selected data with the linear equation.

### 3.3.3 Scanning electron microscopy

Surface morphology and cross-section of triple-cation perovskite solar cells are characterized by a field-emission scanning electron microscope (FESEM; JEOL Model JSM-7001F) and the images are at  $\times 30,000$  magnification.

### 3.3.4 J-V characteristics

The parameters of perovskite solar cells, i.e., power conversion efficiency (PCE), fill factor (FF), short-circuit current ( $J_{SC}$ ), open-circuit voltage ( $V_{OC}$ ), shunt resistance ( $R_{shunt}$ ), and series resistance ( $R_{series}$ ) are investigated from J-V characteristics. The devices are performed under AM1.5 illumination with the light intensity of  $100 \text{ mW/cm}^2$  by using Xe-lamp solar simulator and Keithley 238 source meter-unit at room temperature and the active area of devices is  $0.06 \text{ cm}^2$ .





## Chapter IV

### Results and Discussion

The results of the experiment will be presented in this chapter. The optical transmission and morphology of triple-cation perovskite films fabricated by both methods will be described first. Next, the photovoltaic parameters of triple-cation perovskite solar cells from the conventional two-step deposition method with varied cation ratio will be shown as well as the effect of Br. Then, the performance of FAPbI<sub>3</sub>-based perovskite devices from two-step deposition method with perovskite seeds will be compared to the conventional two-step deposition method. Lastly, the performance from both methods will be in comparison with the standard single-cation perovskite solar cells, MAPbI<sub>3</sub>.

#### 4.1 The optical transmission of perovskite films

The perovskite films are fabricated on the FTO/compact-TiO<sub>2</sub>/mesoporous-TiO<sub>2</sub> by two-step deposition method and two-step deposition method with perovskite seeds. For the conventional method, Cs<sub>0.03</sub>(FA<sub>x</sub>MA<sub>1-x</sub>)<sub>0.97</sub>PbI<sub>3</sub> and Cs<sub>0.03</sub>(FA<sub>x</sub>MA<sub>1-x</sub>)<sub>0.97</sub>Pb(I<sub>0.90</sub>Br<sub>0.10</sub>)<sub>3</sub> are studied and the cation ratio of FA: MA is varied for 90%: 10%, 85%:15%, 70%:30%, 30:70%, 15%:85%, and 10%: 90%. Note that in case of perovskite without halide ions, the band gap of MAPbI<sub>3</sub> is included.

##### 4.1.1 two-step deposition method

Figure 23 shows the optical transmission of different cation ratio perovskite films (a) Cs<sub>0.03</sub>(FA<sub>x</sub>MA<sub>1-x</sub>)<sub>0.97</sub>PbI<sub>3</sub> and (b) Cs<sub>0.03</sub>(FA<sub>x</sub>MA<sub>1-x</sub>)<sub>0.97</sub>Pb(I<sub>0.90</sub>Br<sub>0.10</sub>)<sub>3</sub>. Figure 24 illustrates the relation between  $(\alpha h\nu)^2$  and  $h\nu$  which could be calculated for optical band gap as shown in the table 1 and 2 in which the tables display band gap from each condition of perovskite films without and with 10% bromide, respectively. From the table 1 and 2, band gap is apparently more broaden with the insertion of Br compared to non-Br samples with the same cation ratio. Take one example, the band gap of perovskite sample with cation ratio of FA: MA = 90%: 10% is extended from 1.54 eV to 1.57 eV with the Br-incorporation for only 10%. The altered band gap can be observed with only small amount of Br because perovskite is immensely dominated by the orbitals of the halide ions and Pb<sup>2+</sup> [26]. The conduction band is primarily associated with Pb p orbitals and the valence band is characterized by an antibonding combination of halide ion and Pb orbitals, that is, Pb-6p

and I-5p or Br-4p which mostly influenced by halide ion orbitals. For the insertion of Br into I, the valence band is shifted downward resulting in the wider band gap [27].

Though the band gap is not directly accounted to cations, the band gap slightly lowers as the amount of FA increases, according to table 1 and 2. For instance, the band gap of 1.61 eV reduces to 1.54 eV when FA-content increases from 0% to 90%, corresponding to table 1. This is because the interplay of cation size and hydrogen bonds between organic cation and I ion affect the crystal structure of perovskite materials and the perovskite structure accounts for spin-orbit coupling, namely, the pseudo-cubic of  $FAPbI_3$  enhances the effect of spin-orbit coupling compared to tetragonal with octahedrally tilted of  $MAPbI_3$ . It was found that the band gap of different structure of  $MAPbI_3$  and  $FAPbI_3$  would be the same without spin-orbit coupling effect, and vice versa [8]. According to [8, 28], the increasing band gap was noticed in  $MAPbI_3$  in comparison with  $FAPbI_3$  due to both factors. The change in band gap is compatible with [29] where  $MAPbI_3$  with the introduction of FA and Br was studied. It was found that the band gap was reduced with the incorporation of FA and the band gap was increased with the insertion of Br. Additionally, the band gap trends including the XRD data indicated that FA and Br were homogeneously incorporated into  $MAPbI_3$  lattice and did not observed other segregation perovskite phases except the yellow phase of  $FAPbI_3$  in case of  $FAPbI_3$ -based samples.

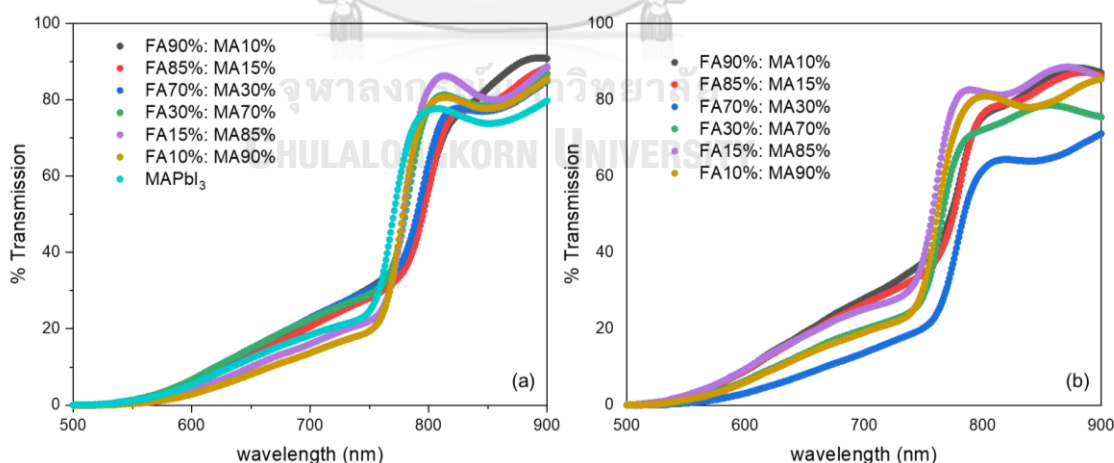


**Figure 23** The optical transmission of triple-cation perovskite films (a)  $Cs_{0.03}(FA_xMA_{1-x})_{0.97}PbI_3$  and (b)  $Cs_{0.03}(FA_xMA_{1-x})_{0.97}Pb(I_{0.90}Br_{0.10})_3$  with different cation ratio.

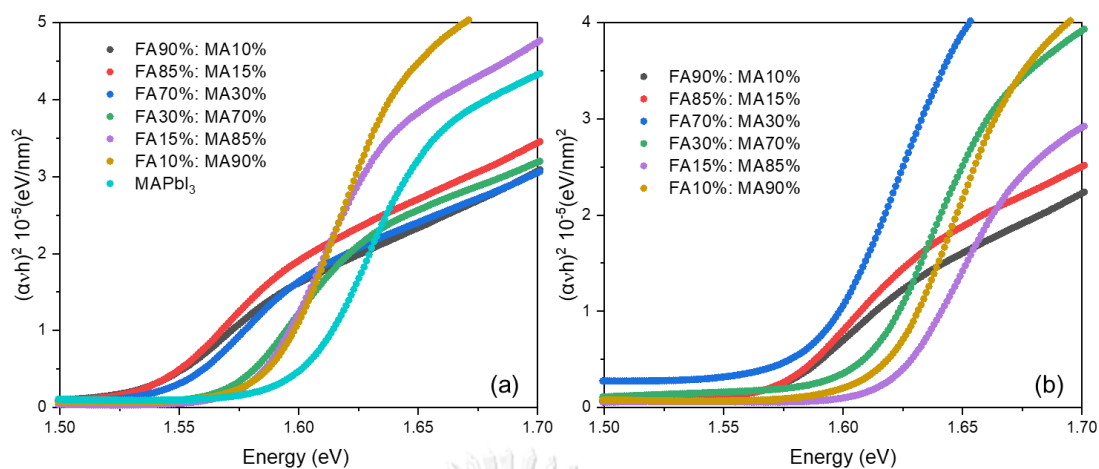


**Figure 24** The relation between  $(\alpha hv)^2$  and  $hv$  where the intercept of  $x$ -axis is the optical band gap of perovskite films (a)  $Cs_{0.03}(F_xMA_{1-x})_{0.97}PbI_3$  and (b)  $Cs_{0.03}(F_xMA_{1-x})_{0.97}Pb(I_{0.90}Br_{0.10})_3$ .

The cation ratio of FA: MA	Band gap (eV)
90%: 10%	$1.54 \pm 0.01$
85%: 15%	$1.54 \pm 0.01$
70%: 30%	$1.55 \pm 0.00$
30%: 70%	$1.58 \pm 0.00$
15%: 85%	$1.59 \pm 0.01$
10%: 90%	$1.60 \pm 0.01$
0%: 100% (MAPbI <sub>3</sub> )	$1.60 \pm 0.01$

**Table 1** The band gap of  $Cs_{0.03}(F_xMA_{1-x})_{0.97}PbI_3$  perovskite films with varied cation ratio.

The cation ratio of FA: MA	Band gap (eV)
90%: 10%	$1.57 \pm 0.00$
85%: 15%	$1.57 \pm 0.01$
70%: 30%	$1.58 \pm 0.01$
30%: 70%	$1.60 \pm 0.01$
15%: 85%	$1.62 \pm 0.01$
10%: 90%	$1.62 \pm 0.00$

**Table 2** The band gap of  $Cs_{0.03}(F_xMA_{1-x})_{0.97}Pb(I_{0.90}Br_{0.10})_3$  perovskite films with varied cation ratio.

#### 4.1.2 two-step deposition method with perovskite seeds

Figure 25 exhibits the optical transmission of perovskite films deposited by two-step deposition method with the seeding concentration of 7, 14, and 20 %v/v. The band gap could be estimated for  $1.56 \pm 0.01$  eV for all seeding concentration which closed to the FAPbI<sub>3</sub>-based samples fabricated by the conventional method. The band gap is not altered as the seeding concentration increases because only the small amount of seeding precursor is concluded compared to the content of primary cations and halide ions.

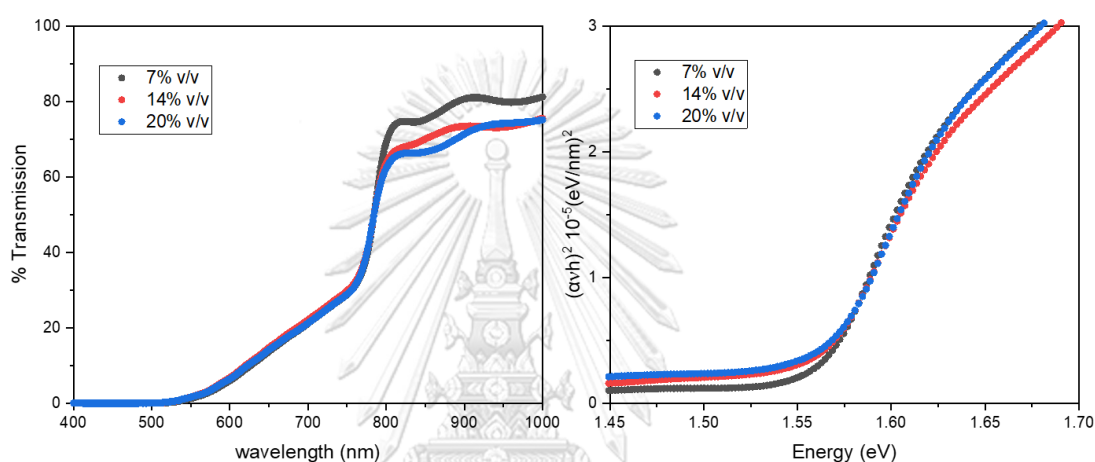


**Figure 25** The optical transmission (left) and the plot of  $(\alpha h\nu)^2$  and  $h\nu$  of perovskite films deposited by two-step deposition method with different seeding concentration (right).

## 4.2 The morphology of perovskite films

The perovskite films are fabricated onto FTO/compact-TiO<sub>2</sub>/mesoporous-TiO<sub>2</sub> by two-step deposition method and two-step deposition method with perovskite seeds. For conventional method, Cs<sub>0.03</sub>(FA<sub>x</sub>MA<sub>1-x</sub>)<sub>0.97</sub>PbI<sub>3</sub> and Cs<sub>0.03</sub>(FA<sub>x</sub>MA<sub>1-x</sub>)<sub>0.97</sub>Pb(I<sub>0.90</sub>Br<sub>0.10</sub>)<sub>3</sub> are studied and the cation ratio of FA: MA is varied for 90%: 10%, 85%:15%, 70%:30%, 30:70%, 15%:85%, and 10%: 90%. The effect of Br is studied as well.

#### 4.2.1 two-step deposition method

- Triple-cation perovskite films without bromide (Cs<sub>0.03</sub>(FA<sub>x</sub>MA<sub>1-x</sub>)<sub>0.97</sub>PbI<sub>3</sub>)

The surfaces of the perovskite films with different cation ratio are shown in figure 26. The grain size of FA-based triple-cation perovskite films is only at 100-150 nm and the spacing between perovskite grains can be clearly observed as shown in figure 26 (a) and (b). As MA-

content increases, the grain orientation is more compact and grain size becomes quite larger as can be seen in figure 26 (e) and (f), though the small-sized grain still takes place.

- Triple-cation perovskite films with 10% bromide ( $\text{Cs}_{0.03}(\text{FA}_x\text{MA}_{100-x})_{0.97}\text{Pb}(\text{I}_{0.90}\text{Br}_{0.10})_3$ )

The results are similar for triple-cation perovskite films with bromide as illustrated in figure 27. The grain size of the perovskite samples with the majority of FA ions is at about 100-150 nm and the spacing still occurs. Additionally, in the case of FA:MA = 15%: 85%, and 10%: 90%, the grain size of 300 nm can be easily spotted and the small-sized grain is barely noticed compared to samples with the absence of bromide from the same cation ratio. So, the inserted bromide might improve the crystallization of perovskite which causes the prominent larger grain size for MA-based perovskite samples. The larger-sized grains observed in MA-based perovskite films after adding Br are in agreement with [29], which was found that the grain size of  $\text{MAPbI}_3$  with the insertion of FA and Br is larger compared to pure  $\text{MAPbI}_3$ . It was surmised that the activation energy for boundary mobility was decreased from the introduction of FA and Br causing the larger grain size and less defected films. The inclusion of Br in FA-based perovskite films does not evidently have effect on the perovskite layer.

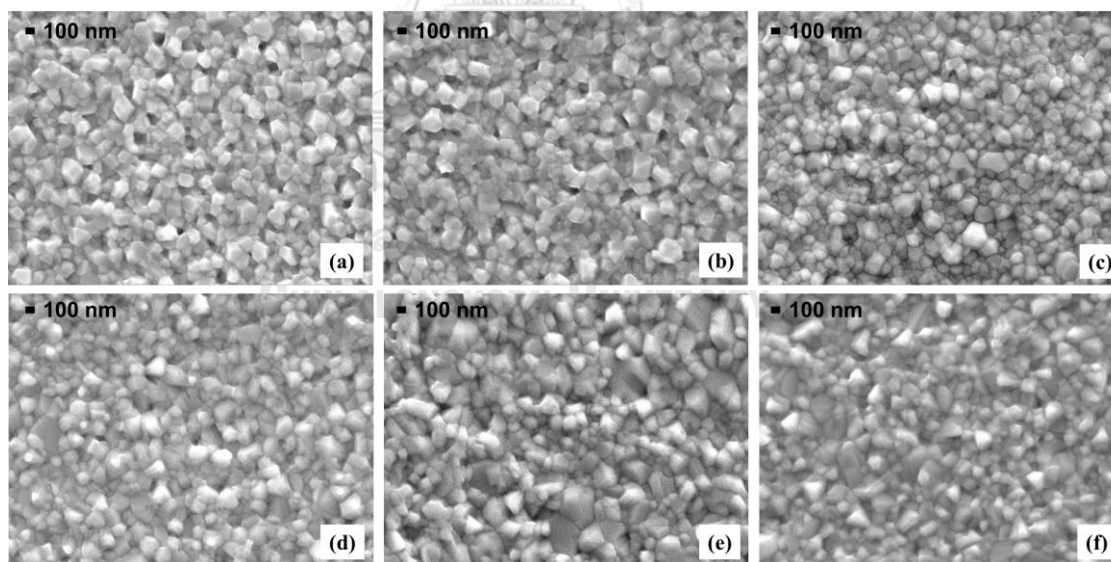


**Figure 26** The SEM images of  $\text{Cs}_{0.03}(\text{FA}_x\text{MA}_{1-x})_{0.97}\text{PbI}_3$  perovskite films with FA: MA cation ratio (a) 90%: 10%, (b) 85%:15%, (c) 70%:30%, (d) 30%:70%, (e) 15%:85%, and (f) 10%: 90% deposited by two-step deposition method.

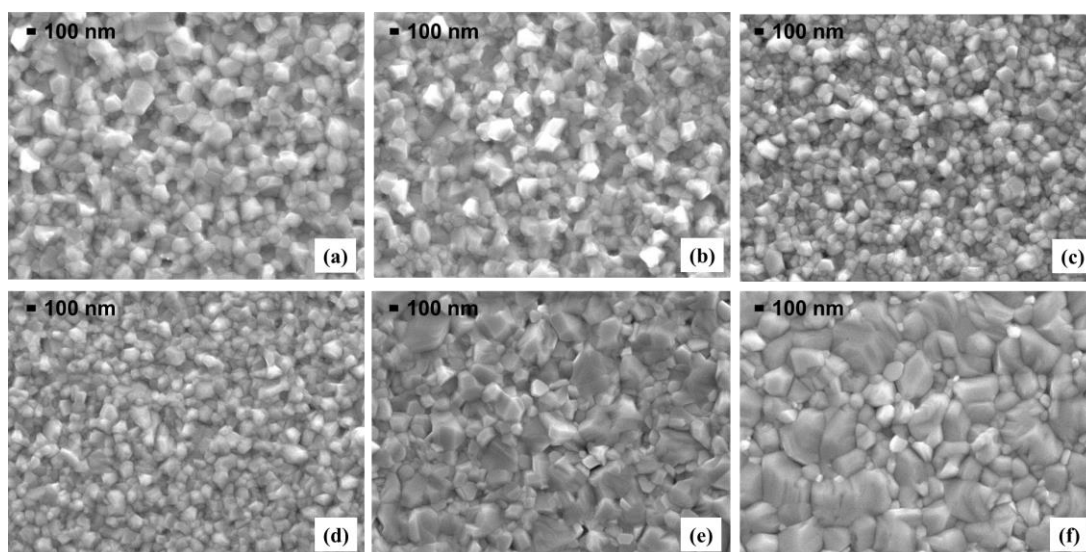


**Figure 27** The SEM images of  $Cs_{0.03}(FA_xMA_{1-x})_{0.97}Pb(I_{0.90}Br_{0.10})_3$  perovskite films with the FA:MA cation ratio (a) 90%:10%, (b) 85%:15%, (c) 70%:30%, (d) 30%:70%, (e) 15%:85%, and (f) 10%:90% deposited by two-step deposition method.

#### 4.2.2 two-step deposition method with perovskite seeds

Since the triple-cation perovskite films deposited from this method are  $FAPbI_3$ -based which is similar to the  $FAPbI_3$ -based perovskite films from the previous method, the grain size and shape are almost the same as shown in figure 28. But the obvious difference is that the resulting films from this method is more compact and denser than the samples fabricated by the conventional method and results in improving the surface coverage for better contact between photoactive layer and hole transport layer. The grain size does not change when the seeding concentration increases because only the small amount of seeds is added as discussed in section 4.1.2.

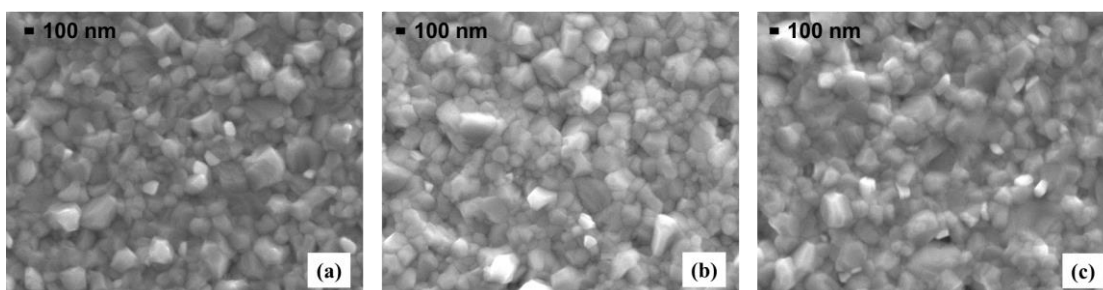


**Figure 28** SEM images of perovskite films fabricated by two-step deposition method with seeding concentration (a) 7% v/v, (b) 14% v/v, and (c) 20% v/v.

### 4.3 The performance of triple-cation perovskite solar cells

In this part, the photovoltaic parameters of devices from the conventional two-step deposition method will be investigated first. Then the performance of devices from the two-step deposition method with perovskite seeds will be compared to the FAPbI<sub>3</sub>-based devices from the old method and the last part is the PCEs from all processes compared to the MAPbI<sub>3</sub> devices.

#### 4.3.1 Two-step deposition method

The table 3 and 4 show the best PCEs of Cs<sub>0.03</sub>(FA<sub>x</sub>MA<sub>1-x</sub>)<sub>0.97</sub>PbI<sub>3</sub> and Cs<sub>0.03</sub>(FA<sub>x</sub>MA<sub>1-x</sub>)<sub>0.97</sub>Pb(I<sub>0.90</sub>Br<sub>0.10</sub>)<sub>3</sub> devices fabricated by the conventional two-step deposition method, respectively. Figure 29 illustrates the plots of JV curves of best PCEs devices.

The cation ratio of FA: MA	PCE (%)	FF	J <sub>SC</sub> (mA/cm <sup>2</sup> )	V <sub>OC</sub> (V)	R <sub>shunt</sub> (Ω·cm <sup>2</sup> )	R <sub>series</sub> (Ω·cm <sup>2</sup> )
90%: 10%	6.68	0.46	14.93	0.97	253.32	3.39
85%: 15%	5.93	0.55	11.74	0.92	238.77	7.96
70%: 30%	4.56	0.54	8.32	1.01	483.19	6.13
30%: 70%	11.84	0.76	15.12	1.03	261.18	3.34
15%: 85%	10.73	0.73	13.74	0.87	597.50	2.99
10%: 90%	16.15	0.67	22.39	1.07	359.67	2.22

**Table 3** The best PCEs of Cs<sub>0.03</sub>(FA<sub>x</sub>MA<sub>1-x</sub>)<sub>0.97</sub>PbI<sub>3</sub> perovskite devices with different cation ratio.

The cation ratio of FA: MA	PCE (%)	FF	J <sub>SC</sub> (mA/cm <sup>2</sup> )	V <sub>OC</sub> (V)	R <sub>shunt</sub> (Ω·cm <sup>2</sup> )	R <sub>series</sub> (Ω·cm <sup>2</sup> )
90%: 10%	5.93	0.54	11.07	0.99	240.96	6.18
85%: 15%	6.39	0.52	12.8	0.96	228.52	9.84
70%: 30%	10.54	0.68	15.10	1.03	682.52	2.66
30%: 70%	13.73	0.60	21.42	1.06	730.08	2.96
15%: 85%	14.65	0.71	18.81	1.09	549.5	2.88
10%: 90%	19.06	0.72	24.16	1.1	397.35	2.87

**Table 4** The best PCEs of Cs<sub>0.03</sub>(FA<sub>x</sub>MA<sub>1-x</sub>)<sub>0.97</sub>Pb(I<sub>0.90</sub>Br<sub>0.10</sub>)<sub>3</sub> perovskite devices with different cation ratio.

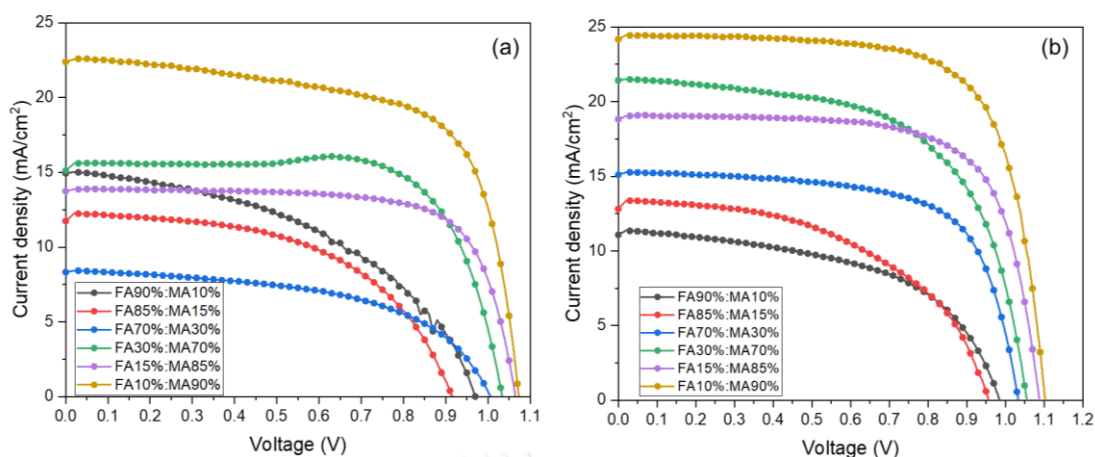


**Figure 29** J-V curves of (a)  $Cs_{0.03}(FA_xMA_{1-x})_{0.97}PbI_3$  and (b)  $Cs_{0.03}(FA_xMA_{1-x})_{0.97}Pb(I_{0.90}Br_{0.10})_3$  devices. The amount of anti-solvent is 50  $\mu$ l and the active area is 0.06  $cm^2$ .

The  $Cs_{0.03}(FA_xMA_{1-x})_{0.97}PbI_3$  devices will be firstly focused. The photovoltaic parameters of the MA-based devices are overall greater than that of the FA-based devices, according to the table 3. Open-circuit voltage of the FA-based devices is slightly lower than that of the MA-based devices due to the red-shifted absorption range. However, the short-circuit current density of FA-based devices is also lower than that of the MA-based devices. It might be because the poor quality of perovskite layer and non-photoactive structure of  $FAPbI_3$  in which its property is not perovskite structure and cannot produce the current. Shunt resistance of FA-based devices is apparently smaller because the spacing of the surface of perovskite films causing defective contact between photoactive layer and HTL, according to SEM images. Series resistance of FA-based devices is quite large because  $FAPbI_3$  might form the yellow phase of  $FAPbI_3$  which is an insulator [15, 30]. Thus, decreased shunt resistance and increased series resistance of FA-based devices lower fill factor.

As a result, the PCEs of the MA-based devices is clearly greater, mostly resulting from low-quality perovskite films, the existence of the yellow phase of  $FAPbI_3$ , and the uneven surface coverage. Note that in the case of  $Cs_{0.03}(FA_{0.30}MA_{0.70})_{0.97}PbI_3$  (green line), although the PCE is quite high, but the characteristic of J-V curve is unusual due to the swollen region which is not a perfect diode characteristic for solar cells.

From the table 4 of  $Cs_{0.03}(FA_xMA_{1-x})_{0.97}Pb(I_{0.90}Br_{0.10})_3$  devices, the photovoltaic parameters tendency for different cation ratio of the Br-containing triple-cation perovskite devices



are very alike to the resulting non-Br devices. The PCEs of FA-based samples are still inferior to that of MA-based devices due to lower short-circuit current density, open-circuit voltage, and series resistance as previously discussed. Interestingly, open-circuit voltage of samples with Br is blatantly better than that of samples without Br since the band gap increases as bromide is introduced. However, short-circuit current density of MAPbI<sub>3</sub>-based devices is also risen comparing to non-Br devices because Br might assist the formation of perovskite films resulting in larger-sized and better-quality grain for MAPbI<sub>3</sub>-based devices. The PCEs from Cs<sub>0.03</sub>(FA<sub>x</sub>MA<sub>1-x</sub>)<sub>0.97</sub>Pb(I<sub>0.90</sub>Br<sub>0.10</sub>)<sub>3</sub> devices are superior to the Cs<sub>0.03</sub>(FA<sub>x</sub>MA<sub>1-x</sub>)<sub>0.97</sub>PbI<sub>3</sub> devices particularly for MAPbI<sub>3</sub>-based devices. Thus, Br might play an important role for photovoltaic performance of MAPbI<sub>3</sub>-based devices due to the improvement of both short-circuit current density and open-circuit voltage. For FAPbI<sub>3</sub>-based with Br-content devices, although the increased open-circuit voltage due to broaden band gap is observed, the other photovoltaic parameters did not clearly improve after the addition of Br. This could be from the poor surface coverage and the yellow phase of FAPbI<sub>3</sub>. From now on, the *FAPbI<sub>3</sub>-based triple-cation perovskite solar cells with Br-content* will be only addressed and called FAPbI<sub>3</sub>-based perovskite solar cells in short.

The results are similar to [29] in which the double-cation perovskite MA<sub>x</sub>FA<sub>1-x</sub>PbI<sub>3</sub> and MA<sub>x</sub>FA<sub>1-x</sub>Pb(I<sub>y</sub>Br<sub>1-y</sub>)<sub>3</sub> devices were investigated. From this study, they showed that the average PCE of the MAPbI<sub>3</sub>-based devices (16.4%) was superior to that of FAPbI<sub>3</sub>-based devices (11.0%) and the PCE of MAPbI<sub>3</sub>-based devices slightly increased after the introduction of 10% Br from 16.4% to 17.3%. It was because the substitution of Br and FA in MAPbI<sub>3</sub> improved the crystallinity of the perovskite films and carrier lifetime.

As described in chapter I, the successful triple-cation perovskite solar cells are mostly FAPbI<sub>3</sub>-based devices but in this study the performance of the FAPbI<sub>3</sub>-based devices are lower than expected especially when compared to [29] where the PCE of double-cation FAPbI<sub>3</sub>-based devices was 11.0%. In addition, the performance of FAPbI<sub>3</sub>-based devices should be higher because of the red-shifted absorption and enhancement of electronic property [14]. To enhance the photovoltaic performance of the FAPbI<sub>3</sub>-based devices, the new approach known as two-step deposition method with perovskite seeds is introduced.

#### 4.3.2 Two-step deposition method with perovskite seeds

This method is focused on improving the PCEs of FAPbI<sub>3</sub>-based perovskite solar cells. In this part, the FAPbI<sub>3</sub>-based device's performance of two-step deposition method with perovskite seeds will be compared to that of the conventional two-step deposition method. The box chart plots of all parameters are shown in figure 31 and the J-V curves of best PCEs of FAPbI<sub>3</sub>-based devices from each condition are plotted in figure 30. The box chart indicates the average of data (the small square box in box plot), the median (the line in box chart), and the distribution of data.

The average short-circuit current density from two-step deposition method with 7% v/v seeding concentration is 18.0 mA/cm<sup>2</sup> and evidently higher than that of the conventional method which is only 13.1 mA/cm<sup>2</sup> for the cation ratio FA:MA = 85%: 15% as shown in figure 31 (c). With almost identical band gap of FAPbI<sub>3</sub>-based perovskite from both methods, the open-circuit voltage is very different, the average open-circuit voltage reaches around 1.05 V for the seeding method. Conversely, the average open-circuit voltage of the conventional method is only 0.92 V. The open-circuit voltage exceeding 1 V indicates that the resulting FAPbI<sub>3</sub>-based perovskite layer is good-quality because the small amount of perovskite seed in PbI<sub>2</sub> could assist the nucleation of perovskite crystals and thus improve the crystal formation of the perovskite layer compared to CsI alone from the conventional method. This also results in the improved short-circuit current density. The reducing of average series resistance from over 19.2 Ω·cm<sup>2</sup> (red box) to only 3.6 Ω·cm<sup>2</sup> (blue box) when changing method from the conventional method to the new one because the non-photoactive phase of FAPbI<sub>3</sub> might be lessened by the seeding technique. In addition, the average shunt resistance of 403 Ω·cm<sup>2</sup> from two-step deposition method with 7%v/v seeding concentration is obtained whereas the average shunt resistance from the conventional method is just 200 Ω·cm<sup>2</sup> resulting from the improved interlayer between perovskite layer and hole transport layer. The decreasing in series resistance and the increasing in shunt resistance translate into the improved average fill factor from about 0.52 of the traditional method to 0.63 of the two-step deposition method with perovskite seeding concentration 7% v/v. Thus, the average PCE of 11.9% obtained from two-step deposition method with 7% v/v seeding concentration is significantly higher than 5.2% of from the conventional method owing to mainly the dense perovskite films and the favor of seeds in helping the crystallization of the black phase of FAPbI<sub>3</sub>.

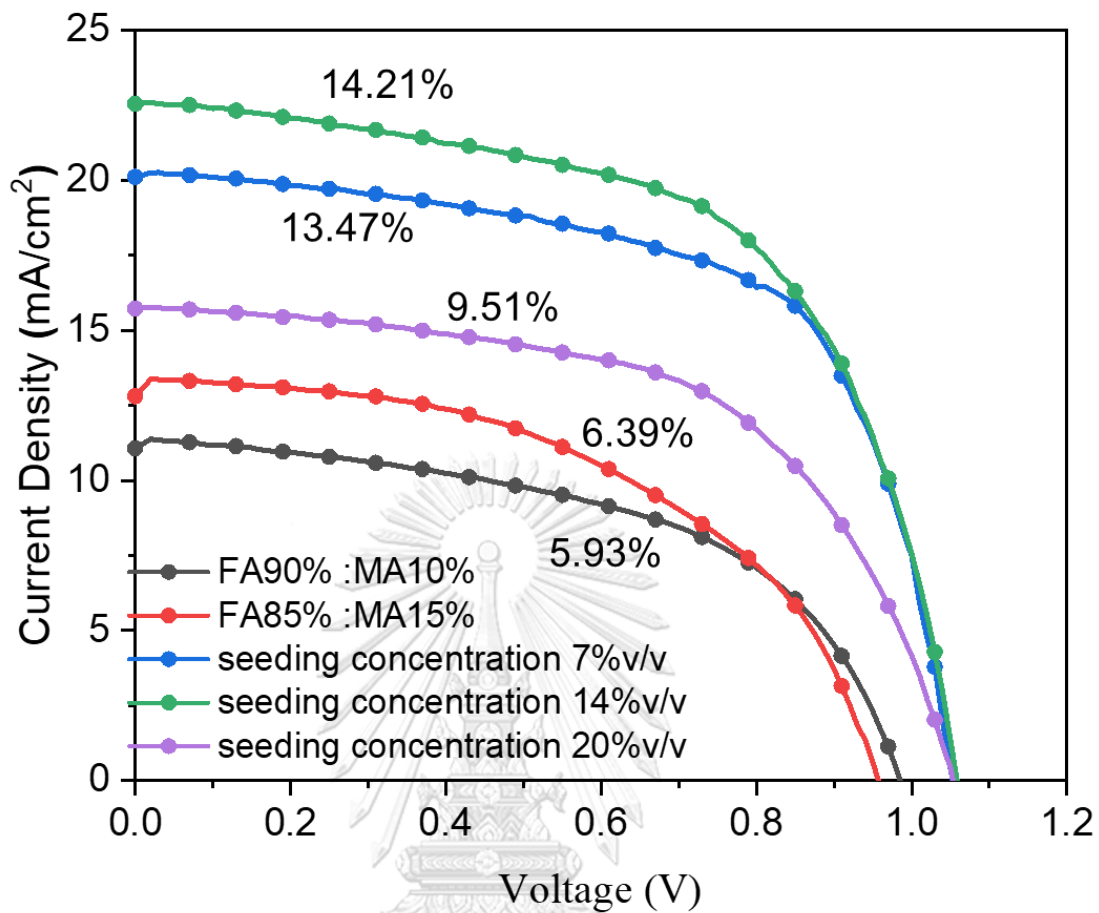


**Figure 30** The  $J$ - $V$  curves of  $FAPbI_3$ -based devices from the conventional method where the cation ratio of FA: MA = 90%: 10% (black line) and 85%: 15% (red line) and the two-step deposition method with perovskite seeding concentration of 7 (blue line), 14 (green line), and 20 (purple line) % v/v. The amount of anti-solvent is 50  $\mu$ l and the active area is 0.06  $cm^2$

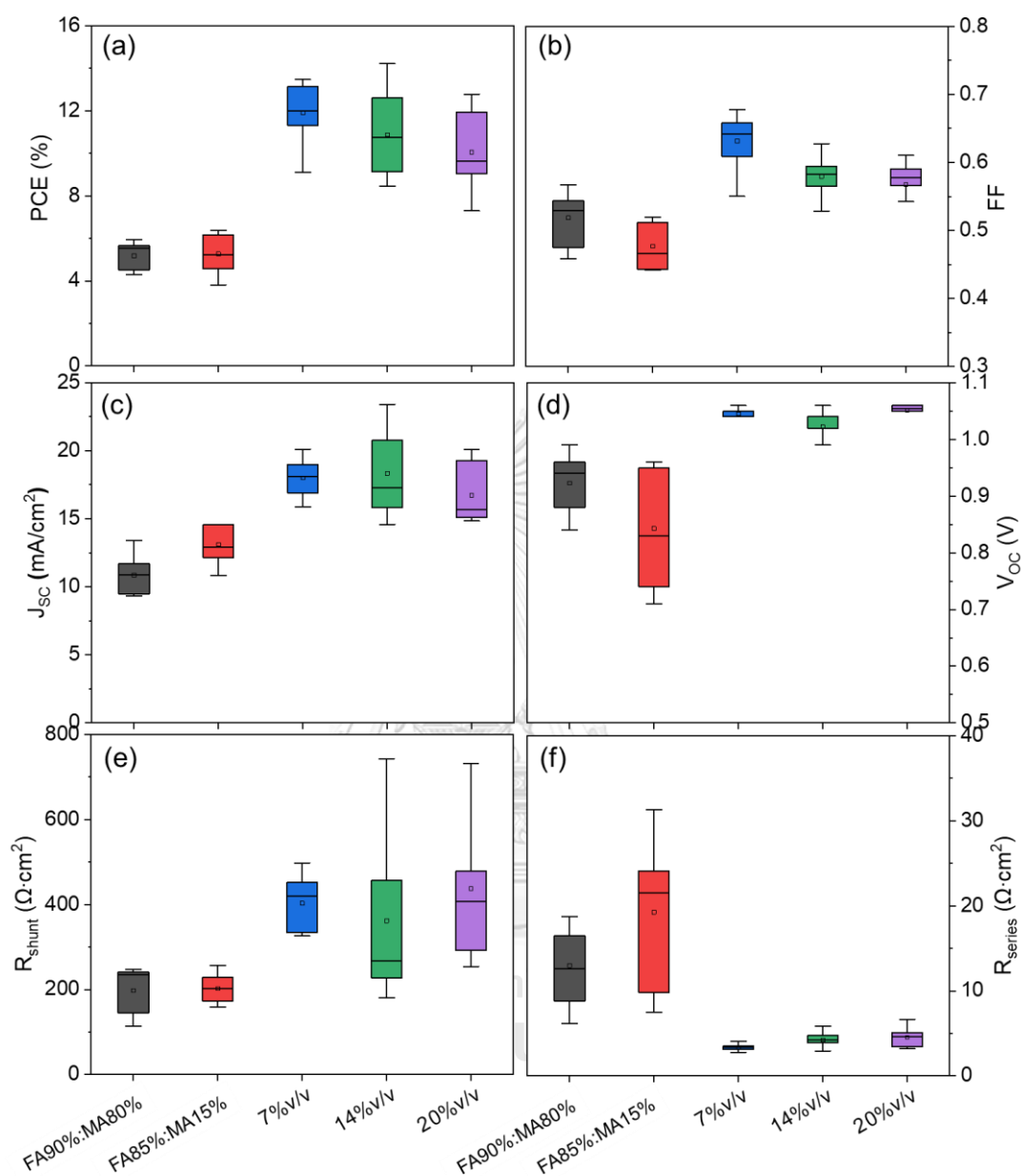


**Figure 31** Box chart plots of solar cell parameters: (a) PCE, (b) FF, (c)  $J_{sc}$ , (d)  $V_{oc}$ , (e)  $R_{shunt}$ , and (f)  $R_{series}$  of FAPbI<sub>3</sub>-based perovskite solar cells fabricated by two-step deposition method with Br-content where cation ratio of FA: MA = 90%: 10% and 85%: 15% and two-step deposition method with perovskite seeds with different seeding concentration. The amount of anti-solvent is 50  $\mu$ l and the active area is 0.06 cm<sup>2</sup>

The effect of the amount of anti-solvent is further studied by using 30, 50, and 100  $\mu\text{l}$  of chlorobenzene as anti-solvent. Figure 32 illustrates the box chart of devices with the amount of anti-solvent.

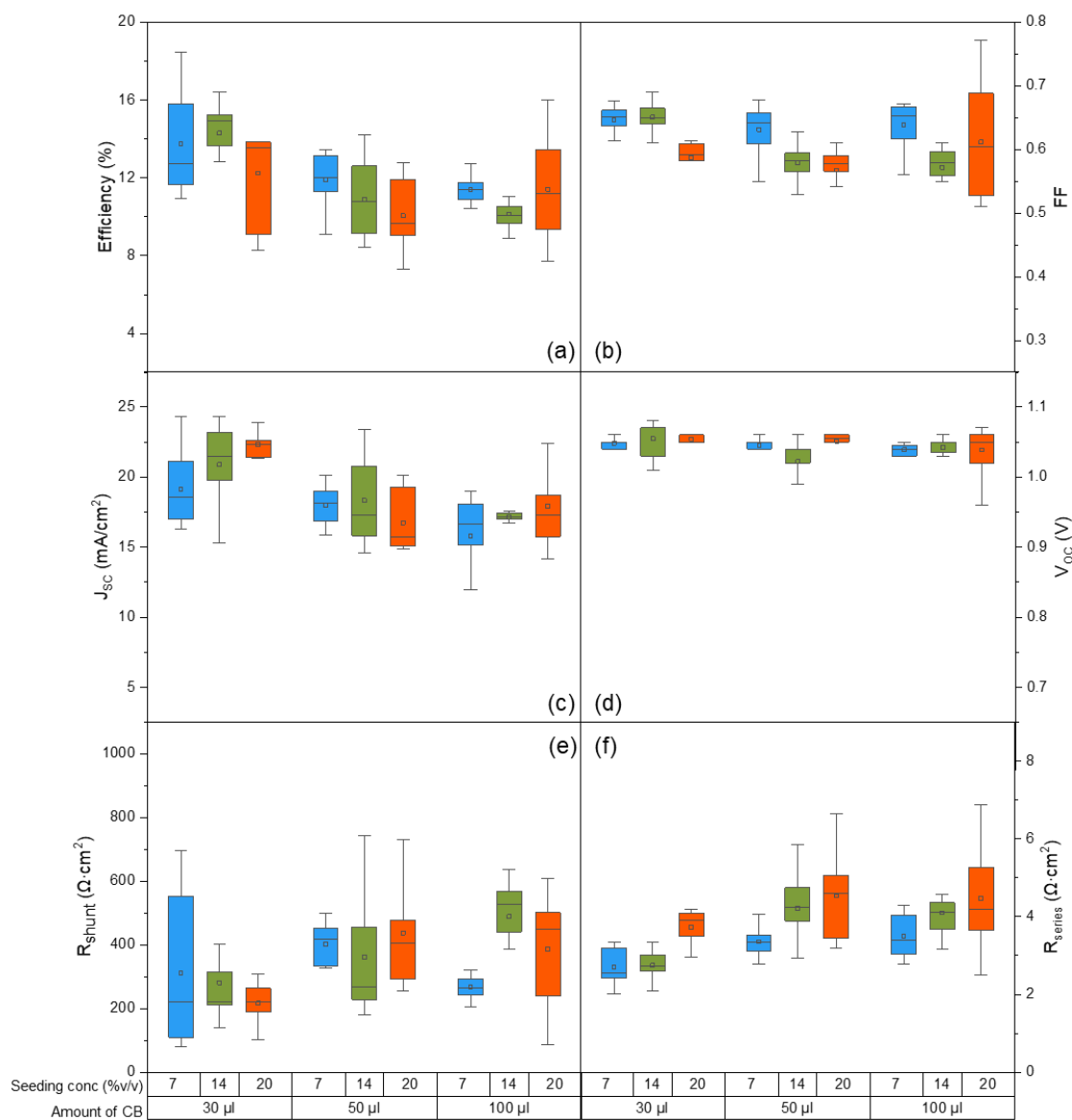


**Figure 32** Box chart plots of parameters: (a) PCE, (b) FF, (c)  $J_{sc}$ , (d)  $V_{oc}$ , (e)  $R_{shunt}$  and (f)  $R_{series}$  of devices fabricated from two-step deposition with seeding concentration of 7 (blue), 14 (green), and 20 (orange) %v/v. The first row is seeding concentration and the second row is the amount of chlorobenzene (CB). The active area is  $0.06 \text{ cm}^2$ .

The average open-circuit voltages from all conditions are similar which is 1.05 eV. Short-circuit current density of devices from 30  $\mu\text{l}$  of chlorobenzene (regardless of seeding concentration) is slightly higher than devices with the amount of anti-solvent 50  $\mu\text{l}$  and 100  $\mu\text{l}$ . For example, the average short-circuit current density is changed from 18.1  $\text{mA}/\text{cm}^2$  to 20.9  $\text{mA}/\text{cm}^2$  for seeding concentration of 14% v/v. Series resistance slightly decreases when anti-solvent of 30  $\mu\text{l}$  is used as well. For instance, the average series resistance of 14% v/v seeding concentration is decreased from 4.2  $\Omega\cdot\text{cm}^2$  to 2.8  $\Omega\cdot\text{cm}^2$  as the content of applied chlorobenzene reduced from 50  $\mu\text{l}$  to 30  $\mu\text{l}$ . However, shunt resistance decreases as the amount of anti-solvent reduced from 50  $\mu\text{l}$  to 30  $\mu\text{l}$ . For instance, the average shunt resistance of 20%v/v seeding concentration is reduced from 438  $\Omega\cdot\text{cm}^2$  to 218  $\Omega\cdot\text{cm}^2$ .

Fill factor of devices from seeding concentration 7 and 20% v/v is significantly unaltered except the fill factor of seeding concentration 14% v/v from 0.57 to 0.65 when reducing the applied chlorobenzene anti-solvent from 50 to 30  $\mu\text{l}$ . The PCEs of devices from this method with any given seeding concentration are enhanced by using 30  $\mu\text{l}$  of anti-solvent. The average PCE of 14% v/v seeding concentration is changed from 10.8% to 14.3% when using 50 and 30  $\mu\text{l}$  of anti-solvent, respectively. The highest PCEs of 18.4% is attained from two-step deposition method with perovskite seeding concentration 7% v/v using 30  $\mu\text{l}$  of anti-solvent. Figure 33 represents a cross-section image of triple-cation perovskite solar cells deposited by such condition.

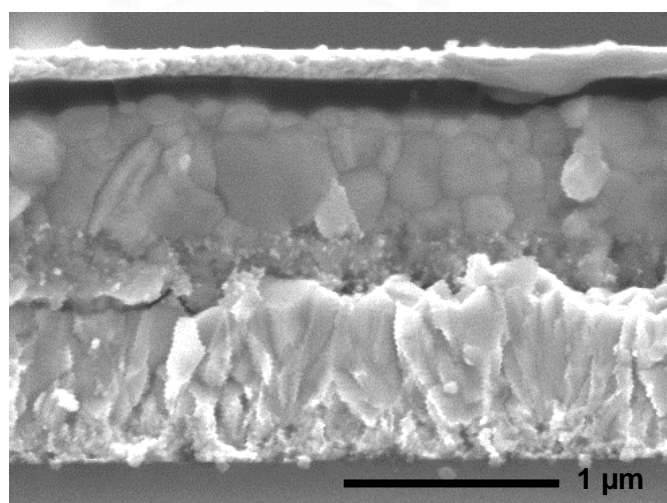


**Figure 33** Cross-section image of a device fabricated by two-step deposition method with seeding concentration 7% v/v and chlorobenzene anti-solvent of 30  $\mu\text{l}$ .

#### 4.3.3 The comparison of devices from all method

Only the  $\text{Cs}_{0.03}(\text{FA}_x\text{MA}_{1-x})_{0.97}\text{Pb}(\text{I}_{0.90}\text{Br}_{0.10})_3$  devices fabricated by two-step deposition method and the cation ratio of 90%: 10%, 85%: 15%, 15%: 85%, and 90%: 10% using 50  $\mu\text{l}$  of anti-solvent including the  $\text{MAPbI}_3$  devices as standard devices will be compared to the  $\text{FAPbI}_3$ -based devices fabricated by two-step deposition method with perovskite seeding concentration 7, 14, and 20%v/v with 30  $\mu\text{l}$  of chlorobenzene anti-solvent. The purpose of this part is to compare the photovoltaic performance of the single-cation perovskite standard devices to the triple-cation perovskite devices from both processes. Figure 34 shows the J-V curves of the best efficiencies from each condition and figure 35 displays the box chart plots of solar cell parameters.

- The average open-circuit voltage is approximately 1.08 V for  $\text{Cs}_{0.03}(\text{FA}_{0.10}\text{MA}_{0.90})_{0.97}\text{Pb}(\text{I}_{0.90}\text{Br}_{0.10})_3$  deposited by two-step deposition method, following by 1.05 V of standard devices and  $\text{FAPbI}_3$ -based devices from the two-step deposition method with 14% v/v seeding concentration. The lower open-circuit voltage compensates the higher average short-circuit current density of 18.4 and 19.1  $\text{mA}/\text{cm}^2$  from standard devices and seeded devices with 14% v/v concentration, respectively, compared to that of 17.6  $\text{mA}/\text{cm}^2$  from  $\text{Cs}_{0.03}(\text{FA}_{0.10}\text{MA}_{0.90})_{0.97}\text{Pb}(\text{I}_{0.90}\text{Br}_{0.10})_3$  deposited by the conventional method.
- For  $\text{FAPbI}_3$ -based devices from the conventional method, the average open-circuit voltage and short-circuit current density are clearly lower than 0.92 V and 13.11  $\text{mA}/\text{cm}^2$ , respectively, due to lower quality perovskite films.
- The average series resistance of  $\text{MAPI}_3$ -based devices, the standard devices, and the seeded devices is only 3  $\Omega\cdot\text{cm}^2$  whereas the average series resistance is almost 20  $\Omega\cdot\text{cm}^2$  in case of  $\text{Cs}_{0.03}(\text{FA}_{0.15}\text{MA}_{0.85})_{0.97}\text{Pb}(\text{I}_{0.90}\text{Br}_{0.10})_3$ . The large series resistance may arise from the yellow phase of  $\text{FAPbI}_3$ .
- The highest average shunt resistance of 409  $\Omega\cdot\text{cm}^2$  is from  $\text{MAPI}_3$ -based devices, following by 364  $\Omega\cdot\text{cm}^2$  of the standard devices, then 310  $\Omega\cdot\text{cm}^2$  of seeded devices. The lowest average shunt resistance of  $\text{FAPbI}_3$ -based devices from the conventional method is below 202  $\Omega\cdot\text{cm}^2$ . It implies that the spacing of the perovskite surface observed in SEM images causes the poor contact between the photoactive layer and hole transport layer.

- The highest average fill factor of 0.71 is obtained from the standard devices and almost equal to the MAPbI<sub>3</sub>-based devices and the fill factor is reduced to 0.65 for seeded devices from the new method. The fill factor of FAPI<sub>3</sub>-based devices from the conventional method is only about 0.48 - 0.52 due to the lower shunt resistance and the larger series resistance.
- The PCE from standard devices, MAPbI<sub>3</sub>-based devices, and seeded devices are able to reach 18%. However, the highest average PCE of 14.3% is obtained from FAPbI<sub>3</sub>-based devices of the seeding method with 14% v/v, following by 14.1% and 13.6% of the MAPbI<sub>3</sub>-based devices from the old method and standard devices, respectively. The average PCE from FAPbI<sub>3</sub>-based devices from the conventional method is only 5.2%.
- Consider the triple-cation perovskite devices fabricated by two-step deposition method. It concurs to the double-cation perovskite devices from [29] where the average PCE of MAPbI<sub>3</sub>-based devices is higher than that of FAPbI<sub>3</sub>-based devices, although the average PCE of MAPbI<sub>3</sub>-based devices of 14.1% from the thesis is slightly lower than that of 17.3% from [29].
- With the assist of seeding method to improve FAPbI<sub>3</sub>-based triple-cation perovskite devices, the average PCE of 14.3% is obtained which is higher than FAPbI<sub>3</sub>-based double-cation perovskite devices [29]. However, it is still inferior to other triple-cation perovskite works. For examples, the average PCEs of FAPbI<sub>3</sub>-based devices fabricated by one-step and two-step deposition method achieved 19.2% [10] and 19.4% [13], respectively.



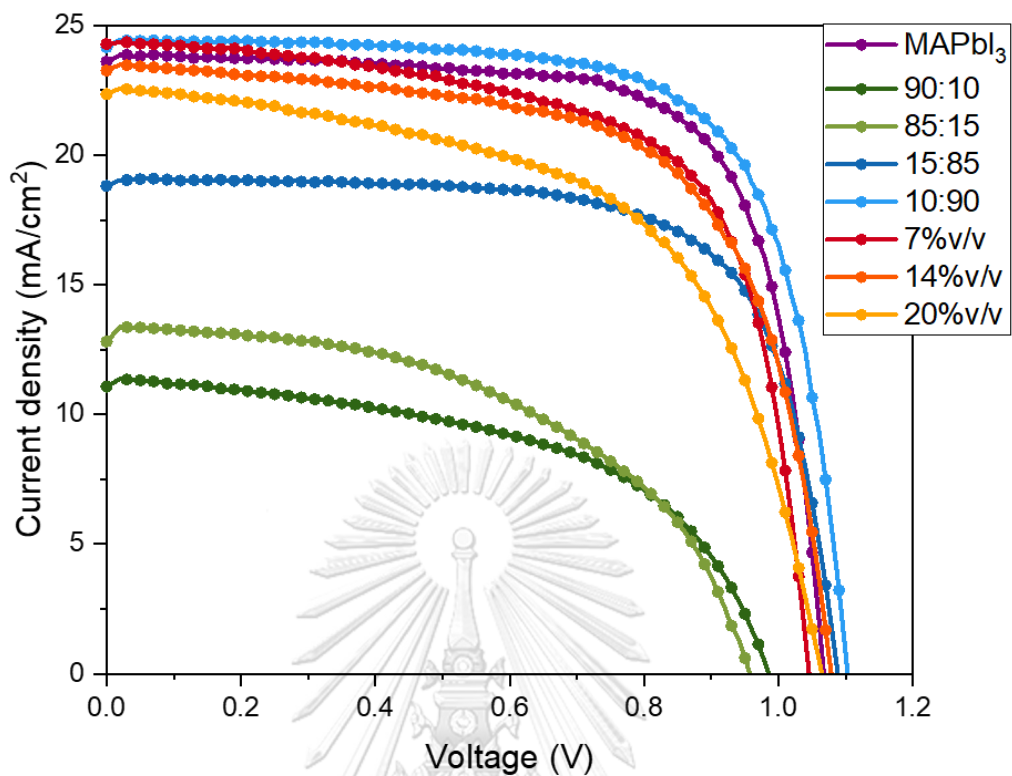


**Figure 34** The  $J$ - $V$  curves of  $\text{MAPbI}_3$  devices (purple),  $\text{Cs}_{0.03}(\text{FA}_x\text{MA}_{1-x})_{0.97}\text{Pb}(\text{I}_{0.90}\text{Br}_{0.10})_3$  solar cells fabricated by two-step deposition method with the FA: MA ratio = 90%: 10% (dark green), 85%:15% (light green), 15%: 85% (dark blue), and 10%: 90% (light blue) using 50  $\mu\text{l}$  of chlorobenzene and two-step deposition method with seeding concentration 7% (red), 14% (orange), and 20% (yellow) v/v and using 30  $\mu\text{l}$  of chlorobenzene. The active area is 0.06  $\text{cm}^2$ .

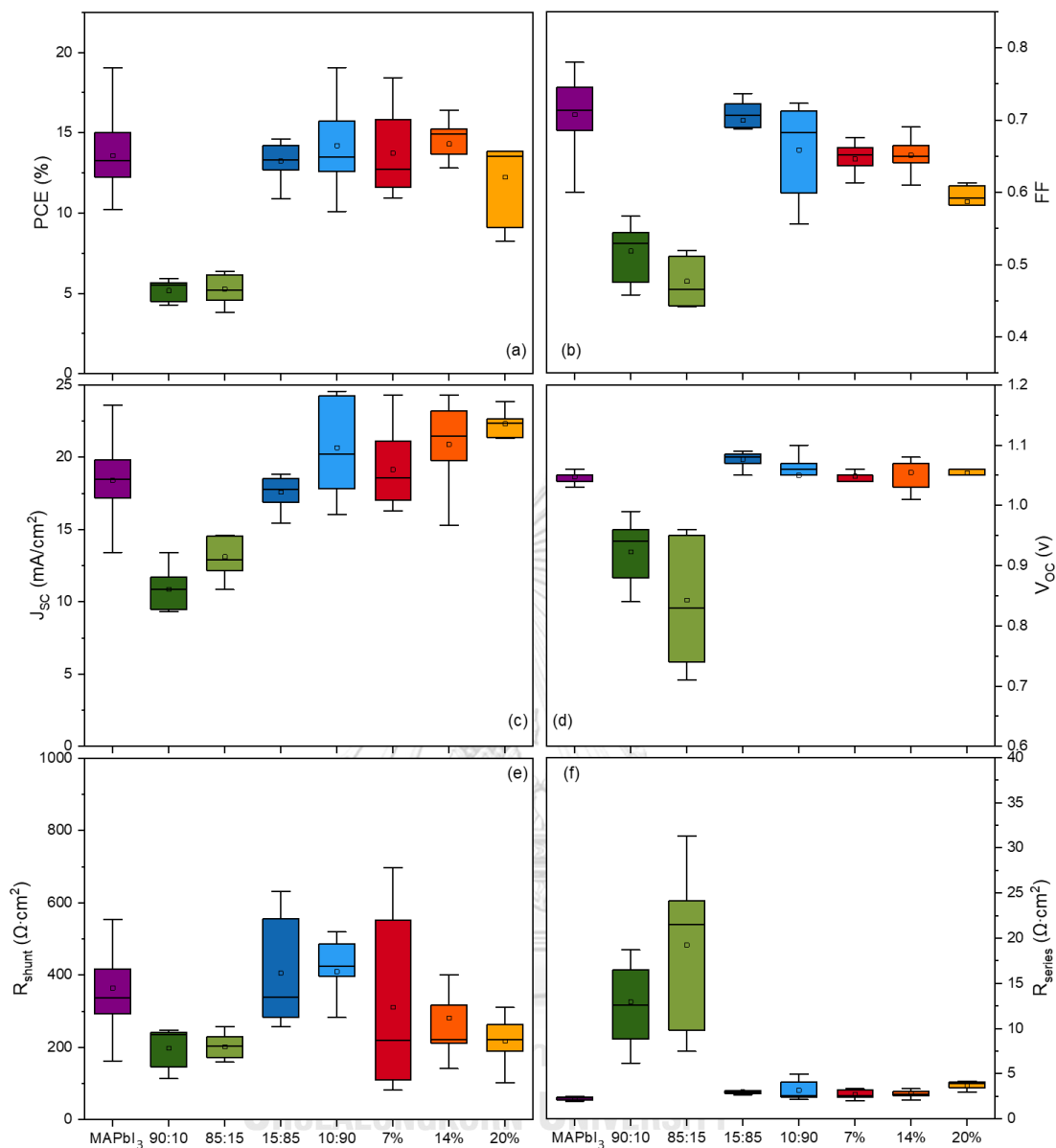


**Figure 35** Box chart plots of the parameters: (a) PCE, (b) FF, (c)  $J_{SC}$ , (d)  $V_{OC}$ , (e)  $R_{shunt}$  and (f)  $R_{series}$  of MAPbI<sub>3</sub> devices (purple),  $Cs_{0.03}(FA_xMA_{1-x})_{0.97}Pb(I_{0.90}Br_{0.10})_3$  solar cells fabricated by two-step deposition method with the FA: MA ratio = 90%: 10% (dark green), 85%:15% (light green), 15%: 85% (dark blue), and 10%: 90% (light blue) using 50  $\mu$ l of chlorobenzene and two-step deposition method with seeding concentration 7% (red), 14% (orange), and 20% (yellow) v/v and using 30  $\mu$ l of chlorobenzene. The active area is 0.06 cm<sup>2</sup>.

## Chapter V

### The conclusions

This work shows the properties of triple-cation perovskite solar cells deposited by two methods. One is the two-step deposition method in which the amount of cation is varied for the ratio of FA: MA = 90%:10%, 85%: 15%, 70%: 30%, 30%: 70%, 15%: 85%, and 10%: 90% and Cs is at 3% of atomic cation. The content of Br is varied as well for 0 and 10% of halide ions. The other method is two-step deposition method with perovskite seeds which is used for FAPbI<sub>3</sub>-based triple-cation perovskite solar cells. The seeding concentration in PbI<sub>2</sub> solution is varied for 7, 14, and 20% v/v, and the amount of chlorobenzene as anti-solvent is also studied.

Firstly, consider the properties of perovskite solar cells fabricated by two-step deposition method. The grain size of perovskite films is increased as the amount of MA and/or Br increases. The optical band gap is evidently wider even the content of Br only increases 10% due to the domination of halide ions and Pb<sup>2+</sup> on the band gap of perovskite materials. Besides, the change of band gap partly reflects on the open-circuit voltage. The open-circuit voltage of Br-contained perovskite devices is higher than that of non-Br perovskite devices. Moreover, the grain size of Br-contained perovskite films is larger particularly MAPbI<sub>3</sub>-based devices. The improved open-circuit voltage and the enlarged grain size could enhance the PCEs. The very small decrease of band gap is observed when the cations are changed from MA to FA because the band gap is not directly subject to the cation. As a result, the open-circuit voltage of FAPbI<sub>3</sub>-based devices is slightly lower than that of MAPbI<sub>3</sub>-based devices.

The short-circuit current density of MAPbI<sub>3</sub>-based devices is higher than that of FAPbI<sub>3</sub>-based devices which contradicts the results of open-circuit voltage. This could be from the appearance of the yellow phase of FAPbI<sub>3</sub> of which the property is an insulator. Moreover, it could be interpreted that the perovskite grains of FAPbI<sub>3</sub> do not have a fine quality since the lower of open-circuit voltage and short-circuit current density are observed. Shunt resistance of FAPbI<sub>3</sub>-devices is lower than that of MAPbI<sub>3</sub>-based devices because of the poor contact of perovskite layer and hole transport layer. Series resistance is still high owing to the yellow phase for FAPbI<sub>3</sub>-based devices. From the increased series resistance and low shunt resistance, fill factor is low for FAPbI<sub>3</sub>-based devices. Thus, the PCEs of FAPbI<sub>3</sub>-based devices are obviously substandard

because (1) the spacing of the perovskite surface and (2) Cs may not facilitate the crystallization of the black phase of FAPbI<sub>3</sub>.

The photovoltaic performance of FAPbI<sub>3</sub>-based triple-cation perovskite devices was not what anticipated. Then, the focus was shifted to improve the quality of FAPbI<sub>3</sub>-based devices. Another approach to fabricate FAPbI<sub>3</sub>-based triple-cation perovskite solar cells was presented, and it was two-step deposition method with perovskite seeds. The optical band gap of seeded samples is similar to that of samples fabricated by the conventional method but the open-circuit voltage of devices from the new method is apparently higher and exceeded 1 V which is almost the same as open-circuit voltage from MAPbI<sub>3</sub>-based devices. Moreover, the short-circuit current density of seeded devices is improved as well. The increase of both open-circuit current density and short-circuit current density indicate that the perovskite films from the new method have better quality compared to the conventional method due to the helping of perovskite seeds to the crystal formation of perovskite films.

According to SEM images, the grain size of FAPbI<sub>3</sub>-based materials from both methods is almost identical but the compactness of perovskite grain is slightly different, the perovskite grain of the new method is denser and more compact than that of the traditional method leading to the improved surface coverage and better contact between perovskite layer and hole transport layer.

In case of two-step deposition method with perovskite seeds, series resistance is very small which is advantageous for fill factor, but the series resistance of the FAPbI<sub>3</sub>-based devices fabricated by the conventional method is still too high due to the yellow phase of FAPbI<sub>3</sub>. Shunt resistance of FAPbI<sub>3</sub>-based devices is increased when using the new method because of the better surface coverage. The amount of anti-solvent was further studied, and it showed that the PCEs slightly improved when using 30  $\mu$ l of chlorobenzene as anti-solvent. However, the effect of chlorobenzene on the optical transmission and SEM images was not observed.

Next, the performance of all conditions and the standard devices is compared. Although, the grain size between FAPbI<sub>3</sub>- and MAPbI<sub>3</sub>-based films is noticeably different, the PCEs from MAPbI<sub>3</sub>-based and standard devices are decent as well as the FAPbI<sub>3</sub>-based devices from the new method. Therefore, the grain size does not crucially play an important role but as to how dense perovskite grain is since the PCEs of FAPbI<sub>3</sub>-based devices actually improve when changing the

approach to seeding method. The films are more compact resulting in greater photovoltaic parameters. Open-circuit voltage and short-circuit current density of FAPbI<sub>3</sub>-based devices are improved by using two-step deposition method with perovskite seeds as well as the lower series resistance. It indicates that seeding precursor is in favor of the subtle forming of crystal perovskite.

Even though FAPbI<sub>3</sub>-based triple-cation perovskite solar cells are more beneficial due to the broaden absorption, this type of perovskite materials is difficult to fabricate and needs more processes to fabricate since it requires the incorporation of perovskite seeds. The PCEs from this seeding method are still similar to the traditional one. In this work, the hysteresis between forward scan and reverse scan is still a huge problem among all perovskite materials even though using mesoscopic structure devices. The mechanism of anti-solvent in two-step deposition method is still unclear. For future work, to improve the performance of PCEs of FAPbI<sub>3</sub>-based triple-cation perovskite solar cells, the concentration of organic cation solution might be one of the big factors that affect the properties of perovskite devices. Moreover, the larger active area for perovskite solar cells is still challenging because the active area for this work is only 0.06 cm<sup>2</sup>.

## REFERENCES

1. *Best Research-Cell Efficiency Chart*. 2020; Available from: <https://www.nrel.gov/pv/cell-efficiency.html>.
2. Cho, A.-N. and N.-G. Park, *Impact of Interfacial Layers in Perovskite Solar Cells*. ChemSusChem, 2017. **10**(19): p. 3687-3704.
3. Kojima, A., et al., *Organometal Halide Perovskites as Visible-Light Sensitizers for Photovoltaic Cells*. Journal of the American Chemical Society, 2009. **131**(17): p. 6050-6051.
4. Conings, B., et al., *Intrinsic Thermal Instability of Methylammonium Lead Trihalide Perovskite*. Advanced Energy Materials, 2015. **5**(15): p. 1500477.
5. Noh, J.H., et al., *Chemical Management for Colorful, Efficient, and Stable Inorganic–Organic Hybrid Nanostructured Solar Cells*. Nano Letters, 2013. **13**(4): p. 1764-1769.
6. Eperon, G.E., et al., *Formamidinium lead trihalide: a broadly tunable perovskite for efficient planar heterojunction solar cells*. Energy & Environmental Science, 2014. **7**(3): p. 982-988.
7. Yang, T.C.-J., et al., *High-Bandgap Perovskite Materials for Multijunction Solar Cells*. Joule, 2018. **2**(8): p. 1421-1436.
8. Anna Amat, E.M., Enrico Ronca, Claudio Quarti†, Paolo Umari, Md. K. Nazeeruddin, Michael Grätzel, and Filippo De Angelis, *Cation-Induced Band-Gap Tuning in Organohalide Perovskites: Interplay of Spin–Orbit Coupling and Octahedra Tilting*. Nano Lett., 2014. **14**(6): p. 3608-3616.
9. Yi, C., et al., *Entropic stabilization of mixed A-cation ABX<sub>3</sub> metal halide perovskites for high performance perovskite solar cells*. Energy & Environmental Science, 2016. **9**(2): p. 656-662.
10. Saliba, M., et al., *Cesium-containing triple cation perovskite solar cells: improved stability, reproducibility and high efficiency*. Energy & Environmental Science, 2016. **9**(6): p. 1989-1997.
11. Li, Z., et al., *Stabilizing Perovskite Structures by Tuning Tolerance Factor: Formation of Formamidinium and Cesium Lead Iodide Solid-State Alloys*. Chemistry of Materials, 2016.

- 28**(1): p. 284-292.
12. Kubicki, D.J., et al., *Phase Segregation in Cs-, Rb- and K-Doped Mixed-Cation (MA)<sub>x</sub>(FA)<sub>1-x</sub>PbI<sub>3</sub> Hybrid Perovskites from Solid-State NMR*. Journal of the American Chemical Society, 2017. **139**(40): p. 14173-14180.
  13. Zhao, Y., et al., *Perovskite seeding growth of formamidinium-lead-iodide-based perovskites for efficient and stable solar cells*. Nature Communications, 2018. **9**(1): p. 1607.
  14. Han, G., et al., *Additive Selection Strategy for High Performance Perovskite Photovoltaics*. The Journal of Physical Chemistry C, 2018. **122**(25): p. 13884-13893.
  15. Zhang, M., et al., *High-Performance Photodiode-Type Photodetectors Based on Polycrystalline Formamidinium Lead Iodide Perovskite Thin Films*. Scientific Reports, 2018. **8**(1): p. 11157.
  16. Simon, S.H., *The Oxford Solid State Basics (First edition.)*. 2013.
  17. Mesquita, I., L. Andrade, and A. Mendes, *Perovskite solar cells: Materials, configurations and stability*. Renewable and Sustainable Energy Reviews, 2018. **82**: p. 2471-2489.
  18. Ravishankar, S., et al., *Influence of Charge Transport Layers on Open-Circuit Voltage and Hysteresis in Perovskite Solar Cells*. Joule, 2018. **2**(4): p. 788-798.
  19. Song, Z., et al., *Pathways toward high-performance perovskite solar cells: review of recent advances in organo-metal halide perovskites for photovoltaic applications*. Journal of Photonics for Energy, 2016. **6**(2): p. 022001.
  20. Tress, W., et al. *The role of the hole-transport layer in perovskite solar cells - reducing recombination and increasing absorption*. in *2014 IEEE 40th Photovoltaic Specialist Conference (PVSC)*. 2014.
  21. Wang, Q., et al., *Recent progress of inorganic hole transport materials for efficient and stable perovskite solar cells*. Nano Select, 2021. **2**(6): p. 1055-1080.
  22. Kato, Y., et al., *Silver Iodide Formation in Methyl Ammonium Lead Iodide Perovskite Solar Cells with Silver Top Electrodes*. Advanced Materials Interfaces, 2015. **2**(13): p. 1500195.
  23. Honsberg, C.B.B.S.G. *Effect of parasitic Resistances*. 2019; Available from: [www.pveducation.org](http://www.pveducation.org).
  24. Singh, R., S. Sandhu, and J.-J. Lee, *Elucidating the effect of shunt losses on the performance of mesoporous perovskite solar cells*. Solar Energy, 2019. **193**: p. 956-961.

25. Tvingstedt, K., et al., *Removing Leakage and Surface Recombination in Planar Perovskite Solar Cells*. ACS Energy Letters, 2017. **2**(2): p. 424-430.
26. Tao, S., et al., *Absolute energy level positions in tin- and lead-based halide perovskites*. Nature Communications, 2019. **10**(1): p. 2560.
27. Meloni, S., et al., *Valence and conduction band tuning in halide perovskites for solar cell applications*. Journal of Materials Chemistry A, 2016. **4**(41): p. 15997-16002.
28. Jono, R. and H. Segawa, *Theoretical Study of the Band-gap Differences among Lead Triiodide Perovskite Materials: CsPbI<sub>3</sub>, MAPbI<sub>3</sub>, and FAPbI<sub>3</sub>*. Chemistry Letters, 2019. **48**(8): p. 877-880.
29. Yang, Z., et al., *Effects of formamidinium and bromide ion substitution in methylammonium lead triiodide toward high-performance perovskite solar cells*. Nano Energy, 2016. **22**: p. 328-337.
30. Xu, X., et al., *Elimination of Yellow Phase: An Effective Method to Achieve High Quality HC(NH<sub>2</sub>)<sub>2</sub>PbI<sub>3</sub>-based Perovskite Films*. ChemSusChem, 2020. **13**(5): p. 956-963.





## Appendix

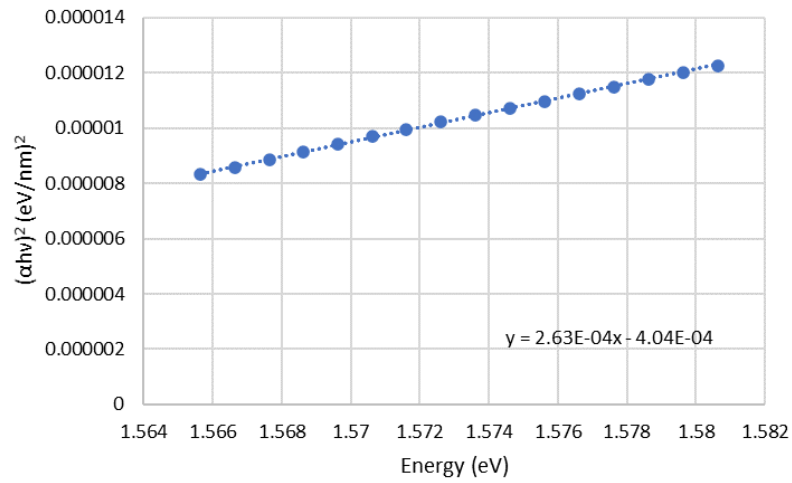


**Figure 36** The plot of  $(\alpha h\nu)^2$  vs energy of  $\text{Cs}_{0.03}(\text{FA}_{0.9}\text{MA}_{0.1})_{0.97}\text{PbI}_3$  with linear equation.

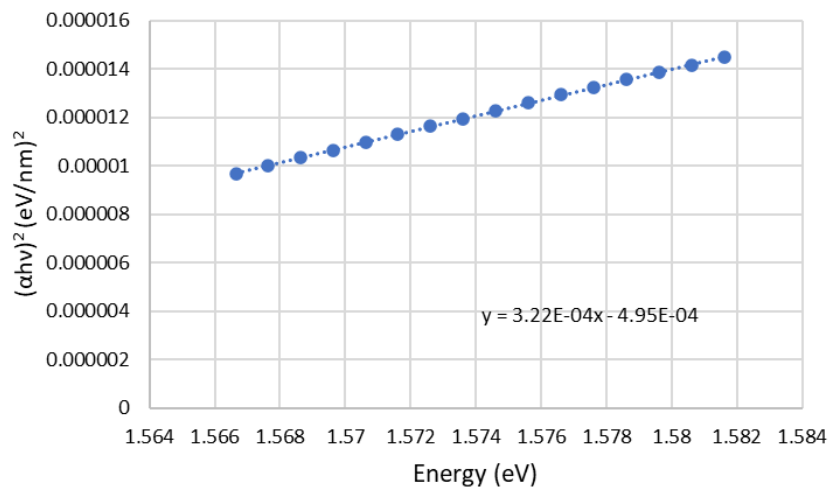


**Figure 37** The plot of  $(\alpha h\nu)^2$  vs energy of  $\text{Cs}_{0.03}(\text{FA}_{0.85}\text{MA}_{0.15})_{0.97}\text{PbI}_3$  with linear equation.

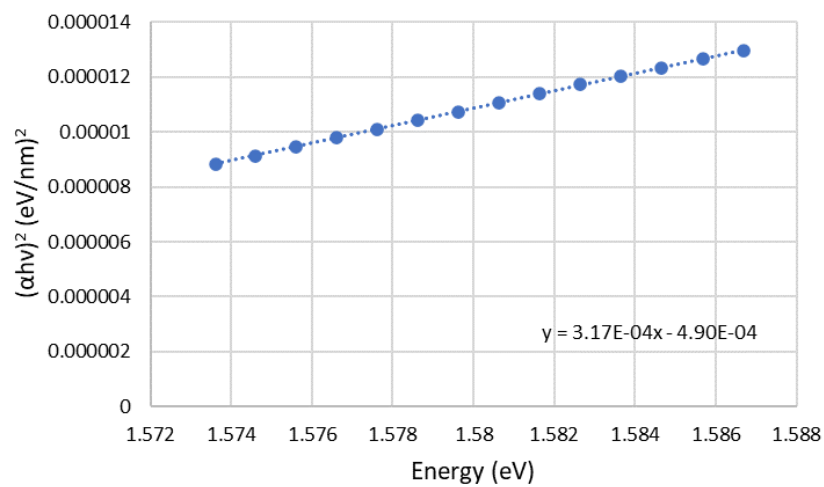


**Figure 38** The plot of  $(\alpha h\nu)^2$  vs energy of  $\text{Cs}_{0.03}(\text{FA}_{0.7}\text{MA}_{0.3})_{0.97}\text{PbI}_3$  with linear equation.

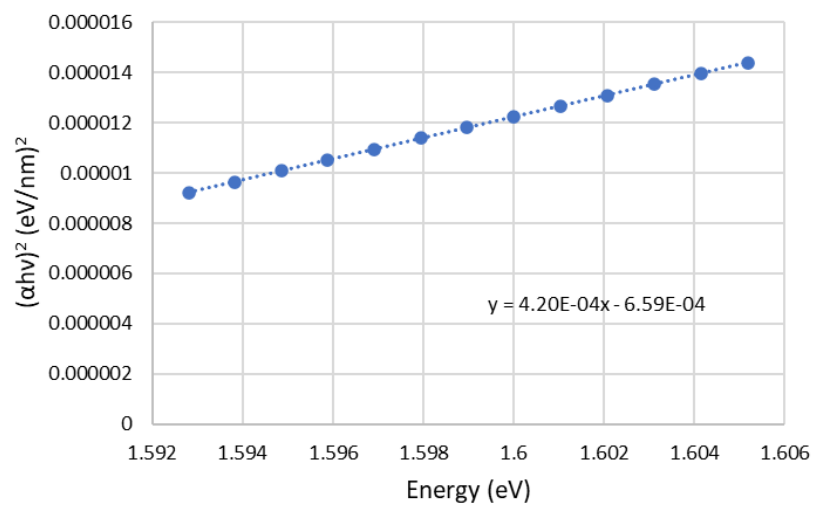


**Figure 39** The plot of  $(\alpha h\nu)^2$  vs energy of  $Cs_{0.03}(FA_{0.3}MA_{0.7})_{0.97}PbI_3$  with linear equation.

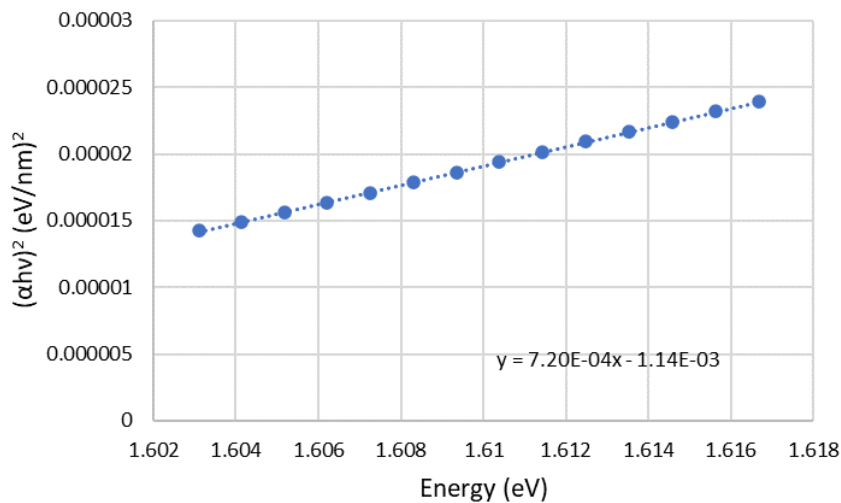


**Figure 40** The plot of  $(\alpha h\nu)^2$  vs energy of  $Cs_{0.03}(FA_{0.15}MA_{0.85})_{0.97}PbI_3$  with linear equation.

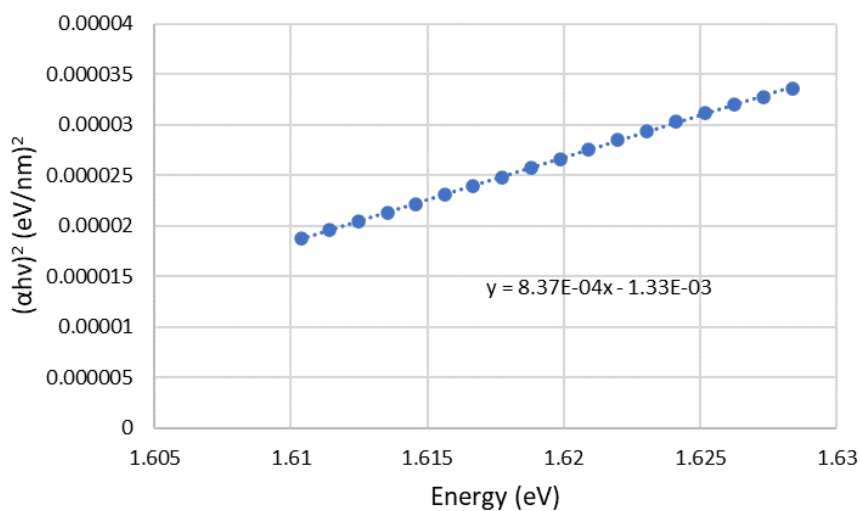


**Figure 41** The plot of  $(\alpha h\nu)^2$  vs energy of  $Cs_{0.03}(FA_{0.1}MA_{0.9})_{0.97}PbI_3$  with linear equation.

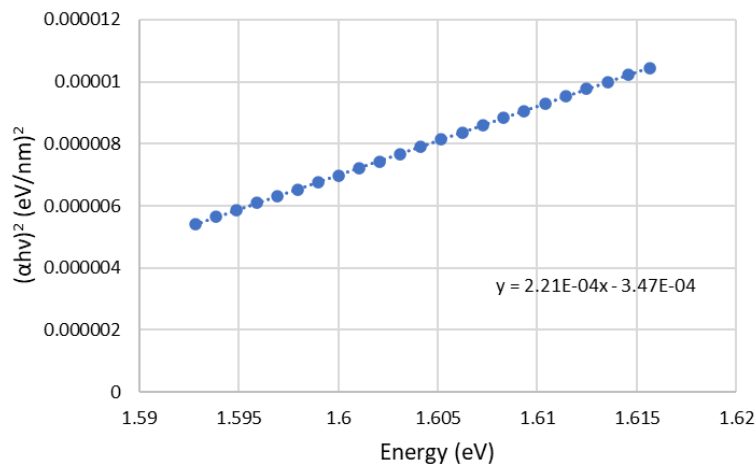


**Figure 42** The plot of  $(\alpha h\nu)^2$  vs energy of  $Cs_{0.03}(FA_{0.9}MA_{0.1})_{0.97}Pb(I_{0.9}Br_{0.1})_3$  with linear equation.

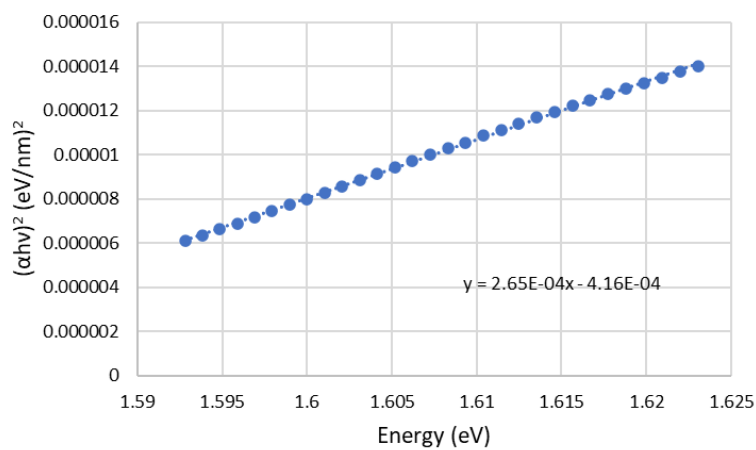


**Figure 43** The plot of  $(\alpha h\nu)^2$  vs energy of  $Cs_{0.03}(FA_{0.85}MA_{0.15})_{0.97}Pb(I_{0.9}Br_{0.1})_3$  with linear equation.

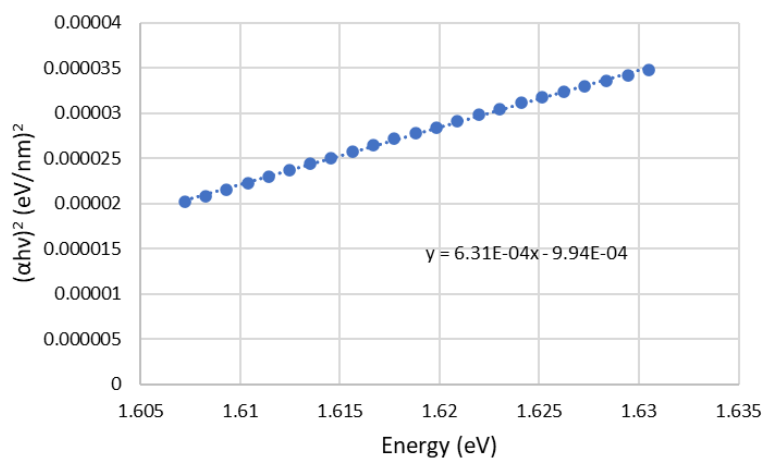


**Figure 44** The plot of  $(\alpha h\nu)^2$  vs energy of  $Cs_{0.03}(FA_{0.7}MA_{0.3})_{0.97}Pb(I_{0.9}Br_{0.1})_3$  with linear equation.

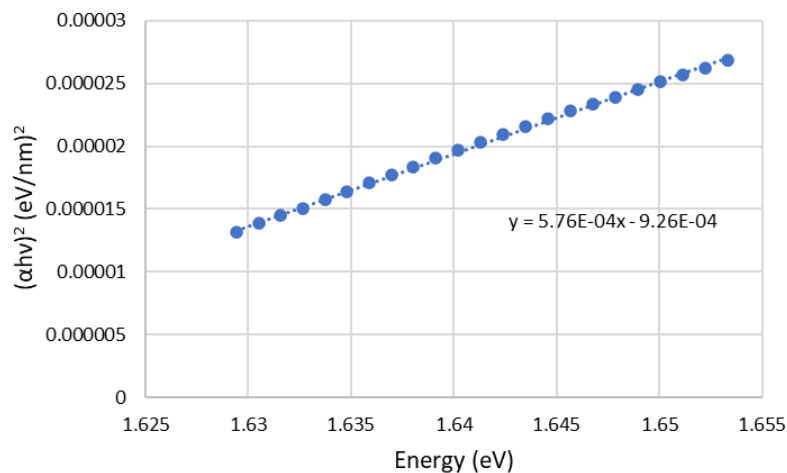


**Figure 45** The plot of  $(\alpha h\nu)^2$  vs energy of  $\text{Cs}_{0.03}(\text{FA}_{0.3}\text{MA}_{0.7})_{0.97}\text{Pb}(\text{I}_{0.9}\text{Br}_{0.1})_3$  with linear equation.

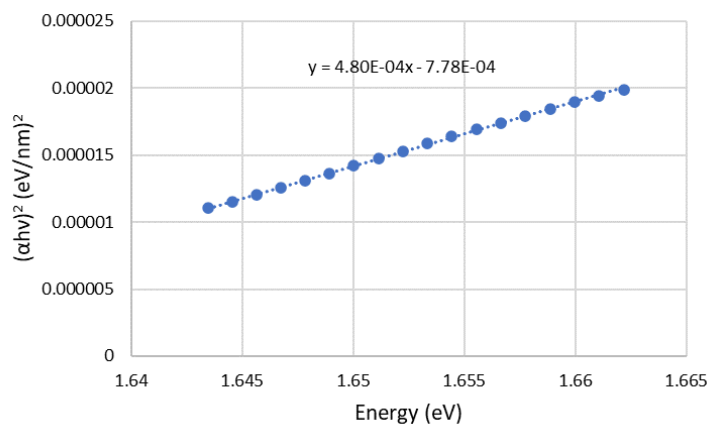


**Figure 46** The plot of  $(\alpha h\nu)^2$  vs energy of  $\text{Cs}_{0.03}(\text{FA}_{0.15}\text{MA}_{0.85})_{0.97}\text{Pb}(\text{I}_{0.9}\text{Br}_{0.1})_3$  with linear equation.

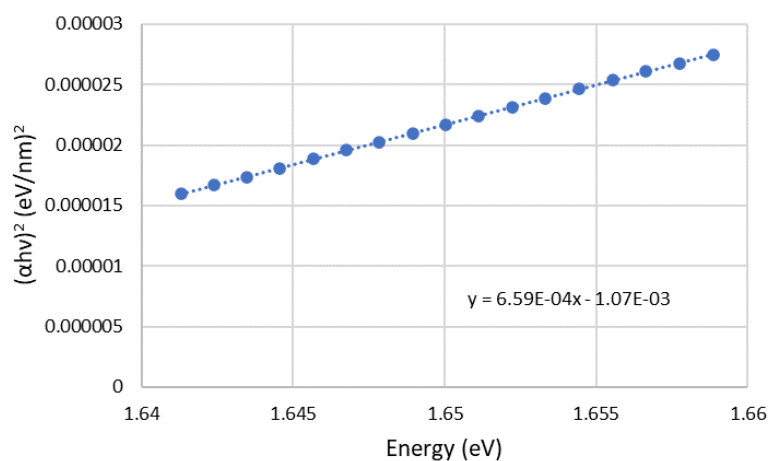


**Figure 47** The plot of  $(\alpha h\nu)^2$  vs energy of  $\text{Cs}_{0.03}(\text{FA}_{0.1}\text{MA}_{0.9})_{0.97}\text{Pb}(\text{I}_{0.9}\text{Br}_{0.1})_3$  with linear equation.

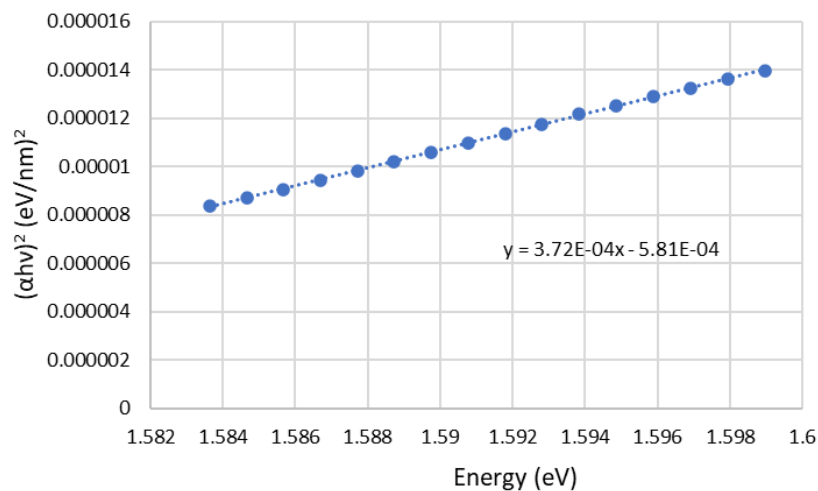


**Figure 48** The plot of  $(\alpha h\nu)^2$  vs energy of the perovskite sample fabricated by two-step deposition method with 7% v/v perovskite seeding concentration.

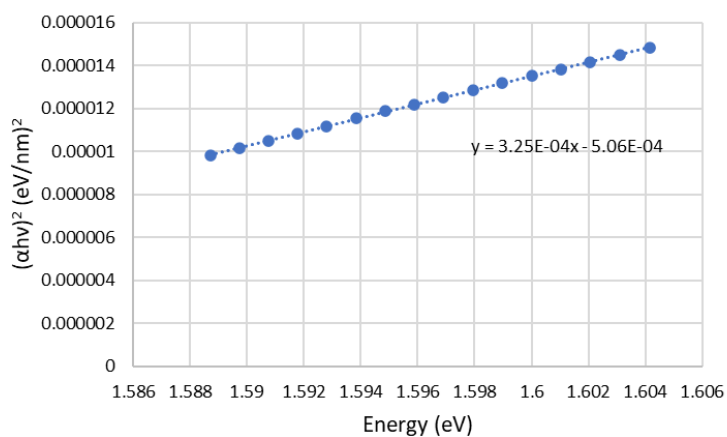


**Figure 49** The plot of  $(\alpha h\nu)^2$  vs energy of the perovskite sample fabricated by two-step deposition method with 14% v/v perovskite seeding concentration.

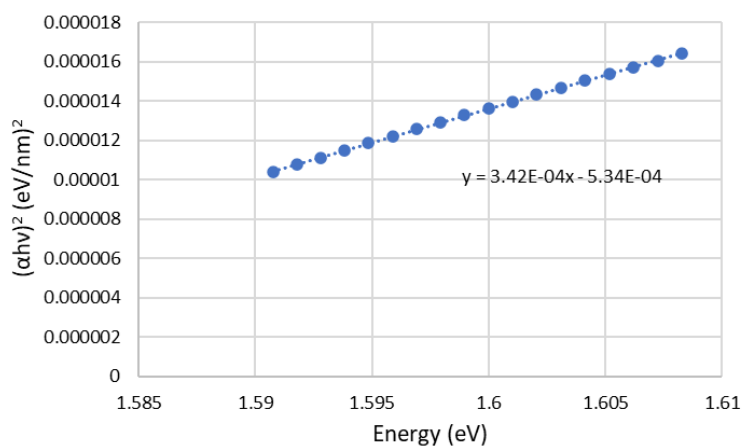


**Figure 50** The plot of  $(\alpha h\nu)^2$  vs energy of the perovskite sample fabricated by two-step deposition method with 20% v/v perovskite seeding concentration.

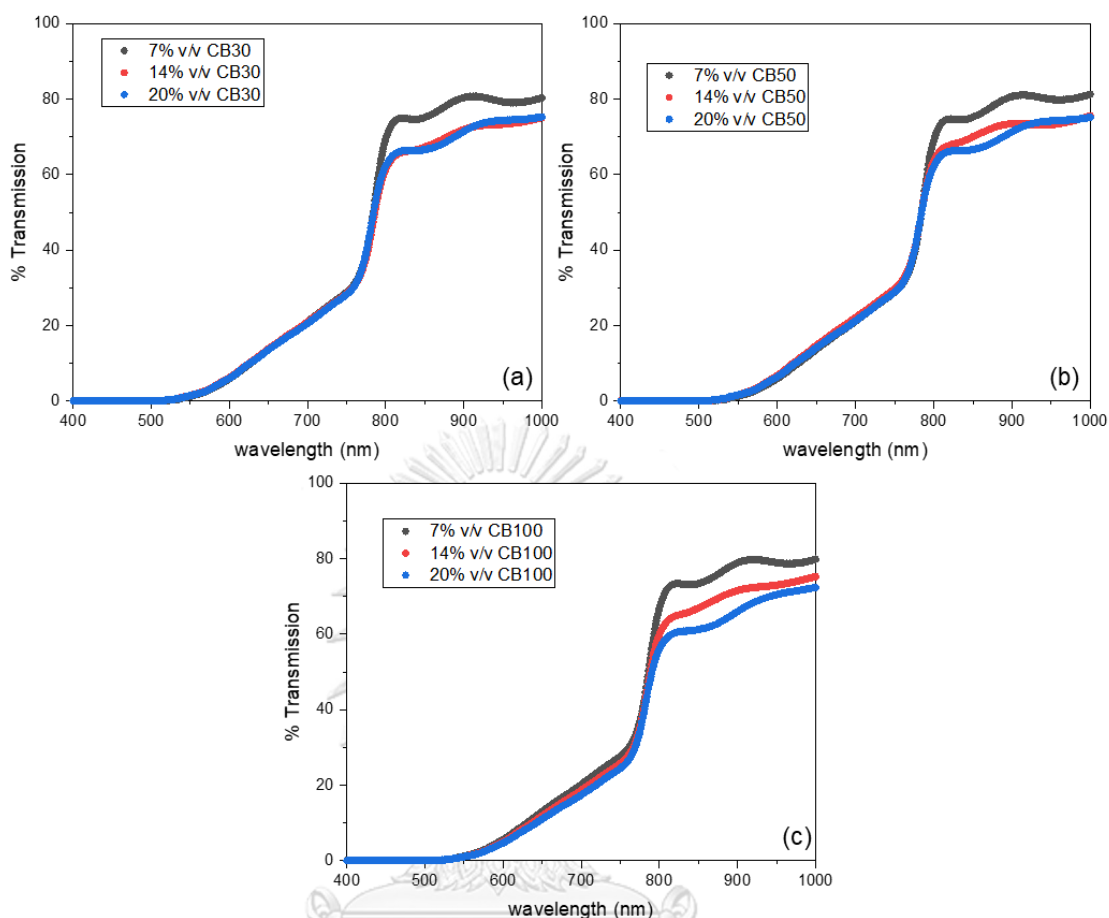


**Figure 51** The optical transmission of triple-cation perovskite films fabricated by two-step deposition method with perovskite seeds. The amount of chlorobenzene is (a) 30 (b) 50 (c) 100  $\mu$ l.

CHULALONGKORN UNIVERSITY

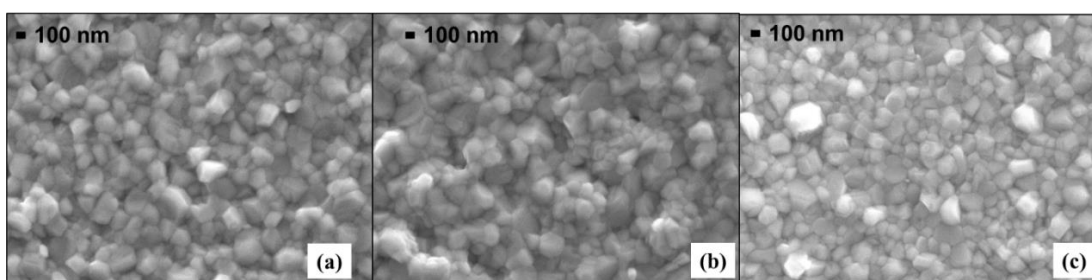


**Figure 52** SEM images of perovskite films fabricated by two-step deposition method with seeding concentration 7% v/v. The amount of chlorobenzene is (a) 30 (b) 50 (c) 100  $\mu$ l.

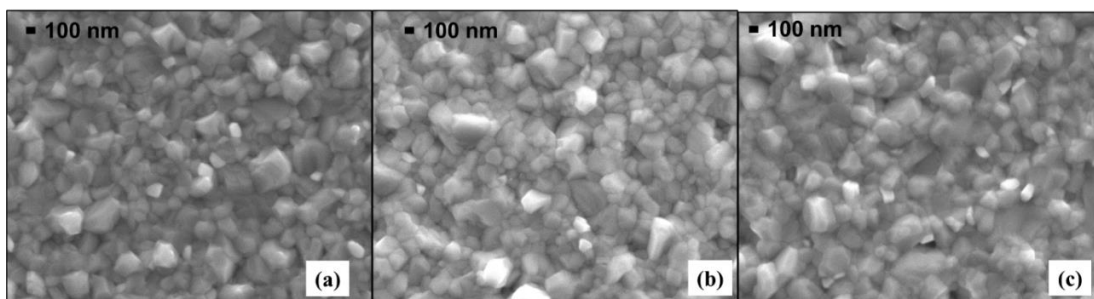


**Figure 53** SEM images of perovskite films fabricated by two-step deposition method with seeding concentration 14% v/v. The amount of chlorobenzene is (a) 30 (b) 50 (c) 100  $\mu$ l.

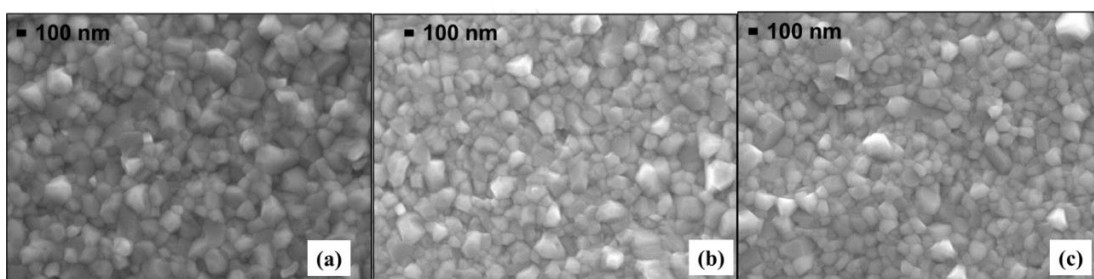


**Figure 54** SEM images of perovskite films fabricated by two-step deposition method with seeding concentration 20% v/v. The amount of chlorobenzene is (a) 30 (b) 50 (c) 100  $\mu$ l.

## VITA

**NAME** Mr. Passakorn Phiromruk

**DATE OF BIRTH** 3 April 1996

**PLACE OF BIRTH** Bangkok

**HOME ADDRESS** 129/5 Tambon Pakpreak, Amphoe Mueng, Kanchanaburi 71000

